

Meteorology of Tropical West Africa: The Forecasters' Handbook

Chapter 2: Synoptic Systems - Lead Authors: R Cornforth, Z Mumba, DJ Parker

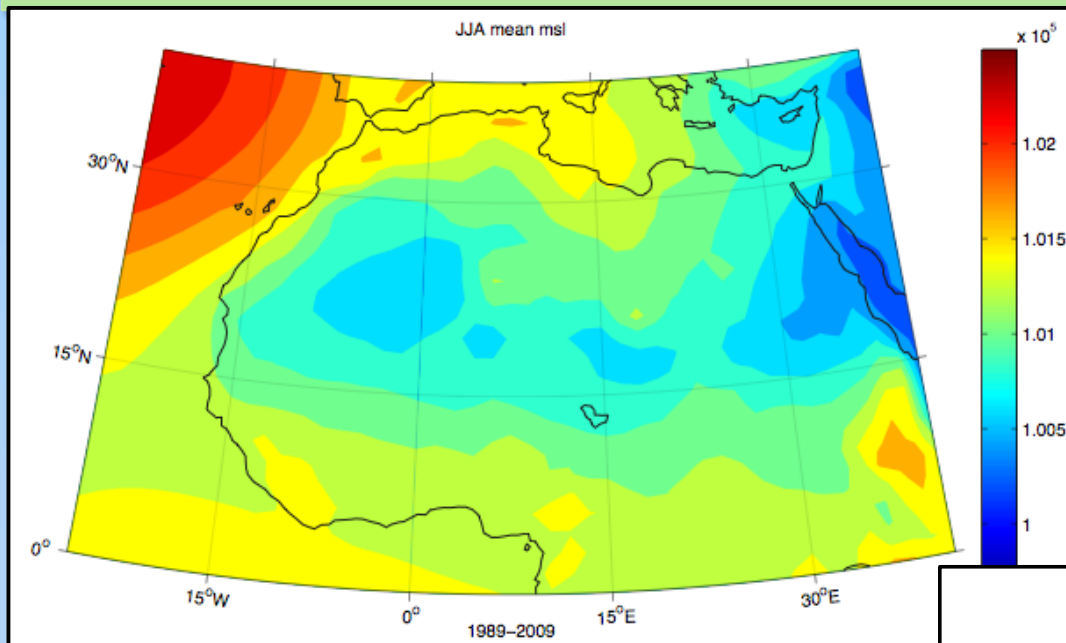
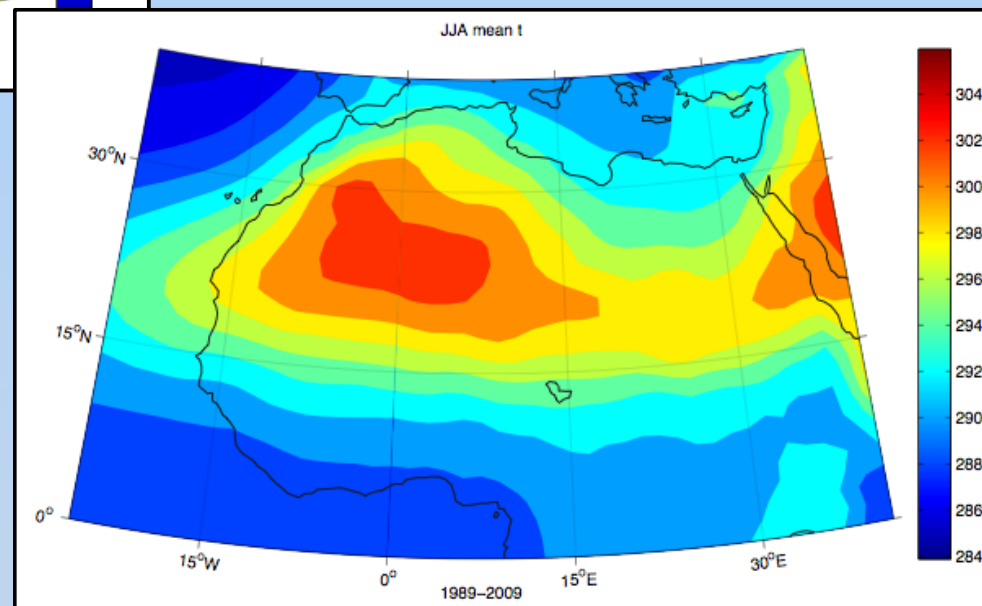


Figure 2.1: Characteristics of the Saharan Heat Low seen in ECMWF ERA Interim climatological mean (1989-2009) fields for June/July/August (JJA) for (a) mean sea level pressure, (b) temperature at 850 hPa.



Meteorology of Tropical West Africa: The Forecasters' Handbook

Chapter 2: Synoptic Systems - Lead Authors: R Cornforth, Z Mumba, DJ Parker

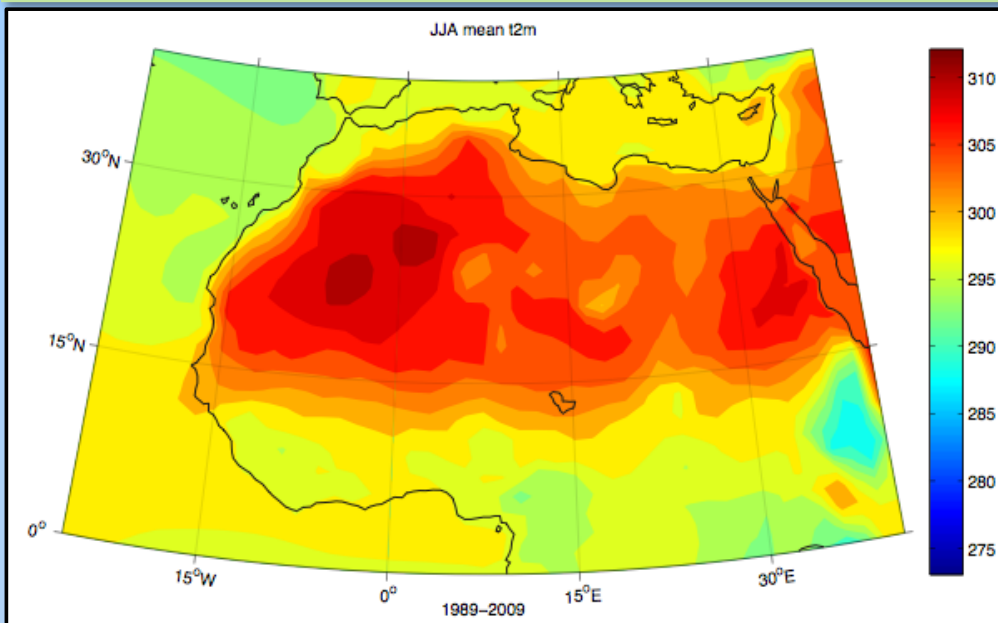
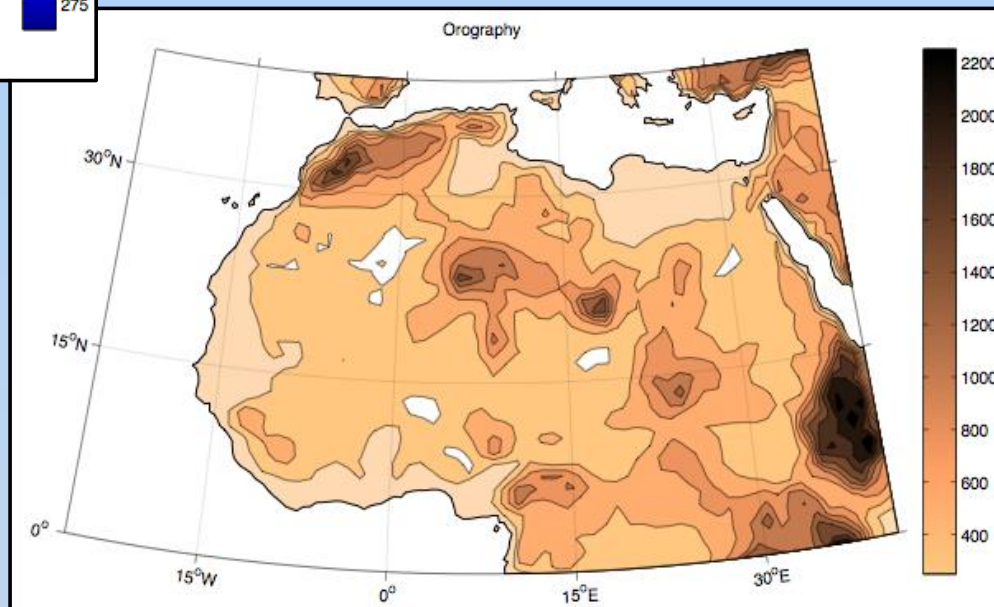


Figure 2.1: Characteristics of the Saharan Heat Low seen in ECMWF ERA Interim climatological mean (1989-2009) fields for June/July/August (JJA) for (c) 2 metre temperature and (d) orographic height.



Meteorology of Tropical West Africa: The Forecasters' Handbook

Chapter 2: Synoptic Systems - Lead Authors: R Cornforth, Z Mumba, DJ Parker

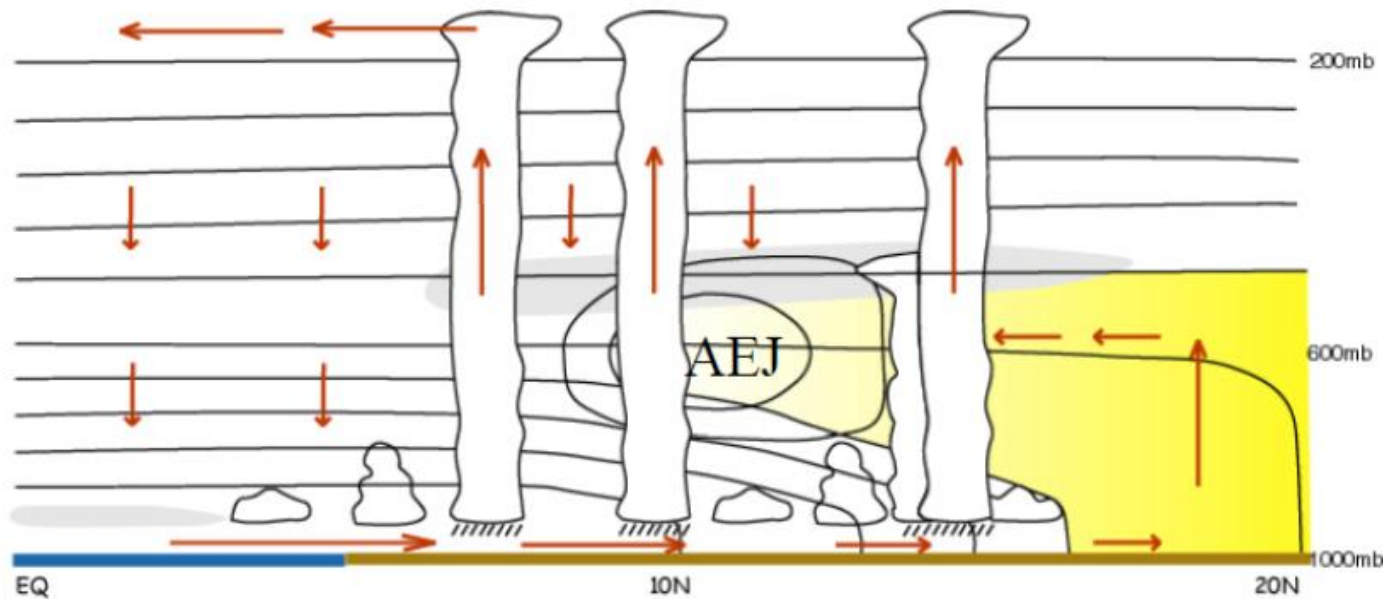
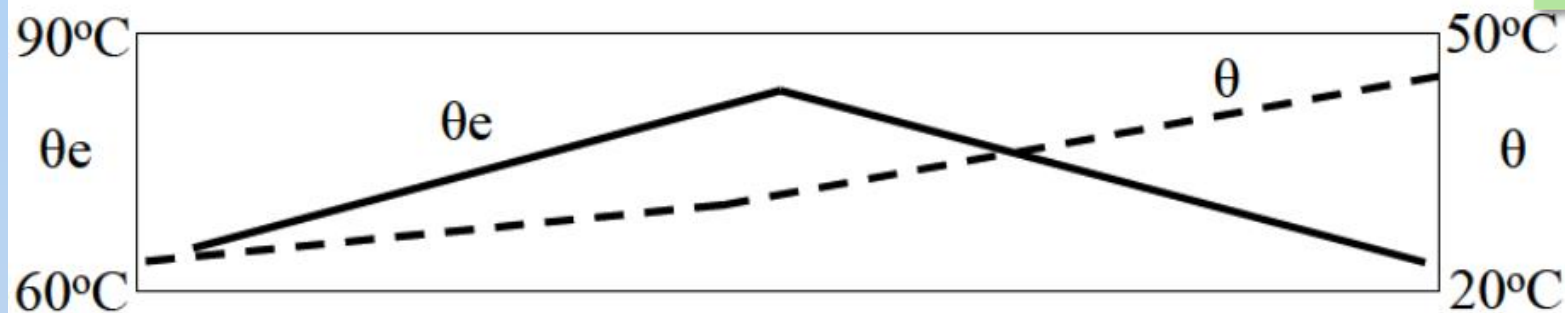


Figure 2.2: Schematic south-north vertical cross-section along the Greenwich Meridian, highlighting the Saharan heat low-AEJ-ITCZ system and SAL (shaded yellow), with meridional variations in atmospheric boundary layer potential temperature (θ ; contoured in upper panel) and equivalent potential temperature (θ_e).



The monsoon trough is located just to the south of the AEJ. Adapted from Figure 10 of Parker et al. (2005a) for the AMMA International Science Plan (http://amma-international.org/library/docs/AMMA_ISP_May2005.pdf), and to be compared with Figures 1.1 and 1.34.

Meteorology of Tropical West Africa: The Forecasters' Handbook

Chapter 2: Synoptic Systems - Lead Authors: R Cornforth, Z Mumba, DJ Parker

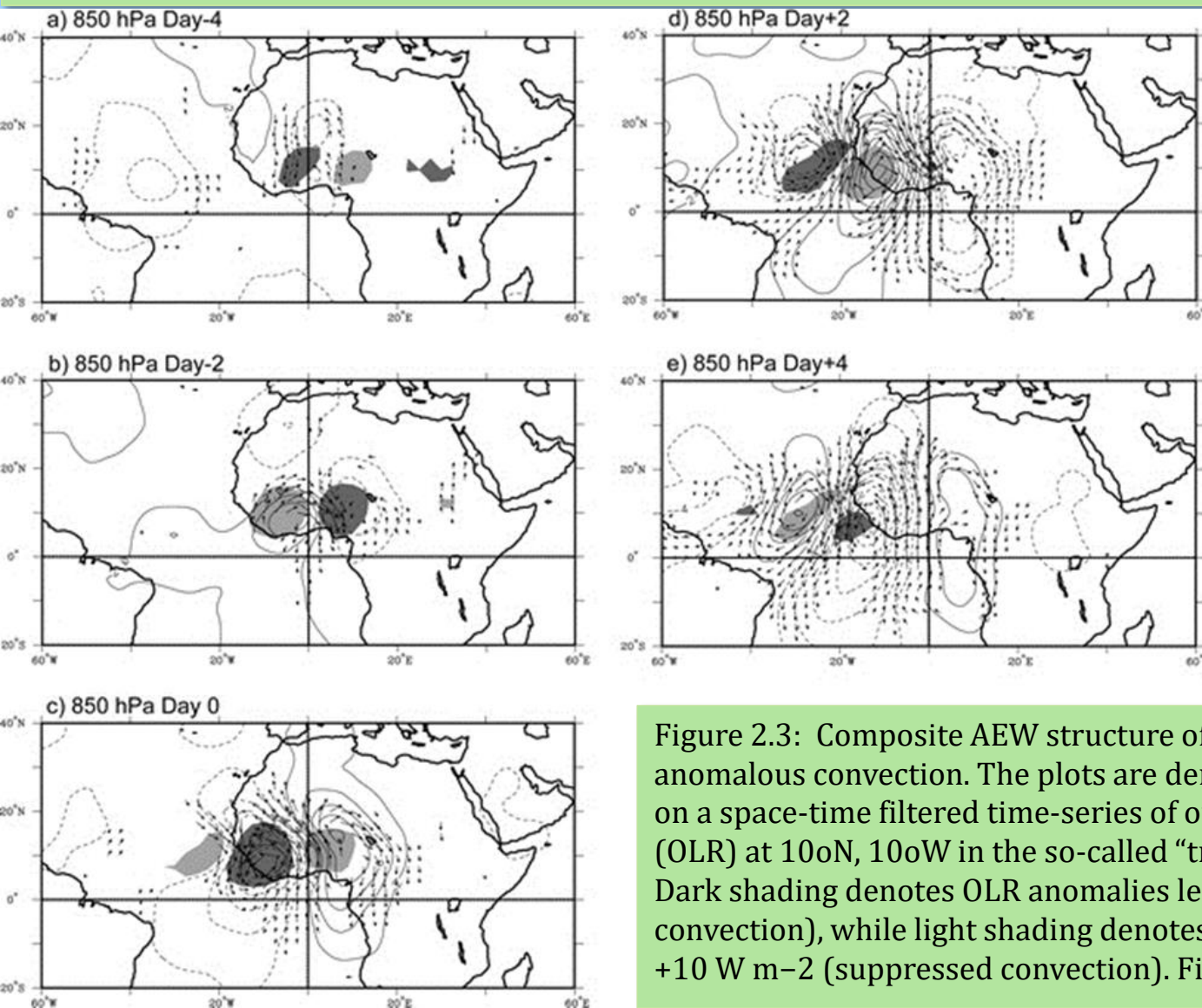


Figure 2.3: Composite AEW structure of 850 hPa streamfunction with anomalous convection. The plots are derived from a regression based on a space-time filtered time-series of outgoing long-wave radiation (OLR) at 10oN, 10oW in the so-called “tropical depression” band. Dark shading denotes OLR anomalies less than -10 W m^{-2} (active convection), while light shading denotes OLR anomalies greater than $+10 \text{ W m}^{-2}$ (suppressed convection). Fig 3 from Kiladis et al. (2006).

Meteorology of Tropical West Africa: The Forecasters' Handbook

Chapter 2: Synoptic Systems - Lead Authors: R Cornforth, Z Mumba, DJ Parker

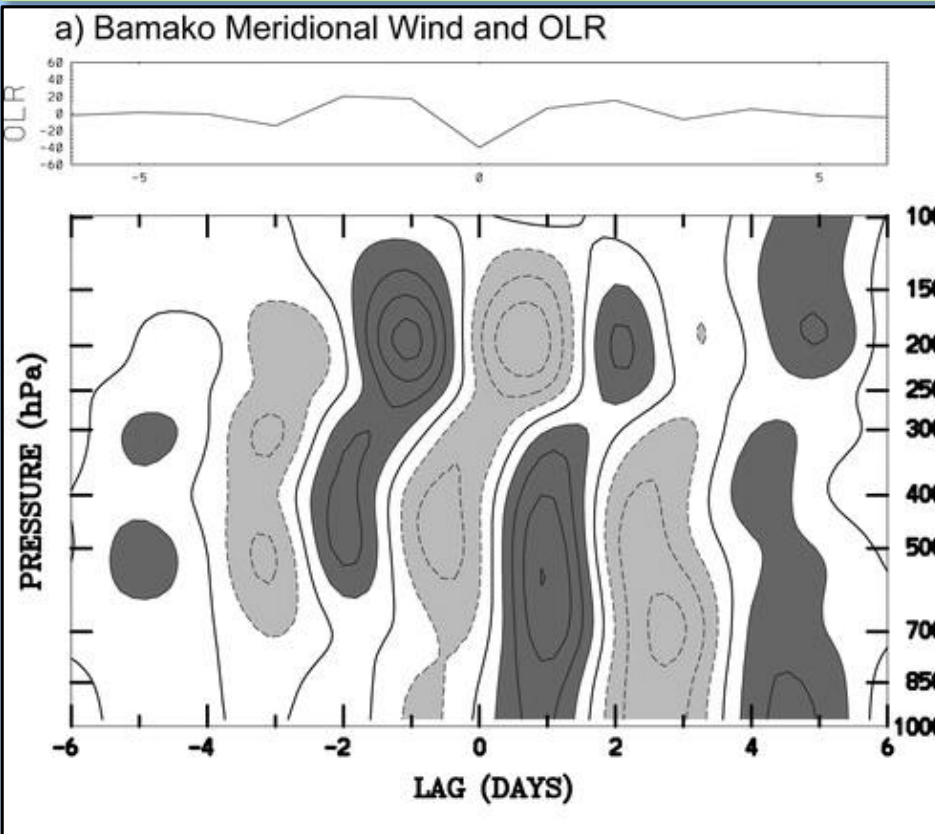
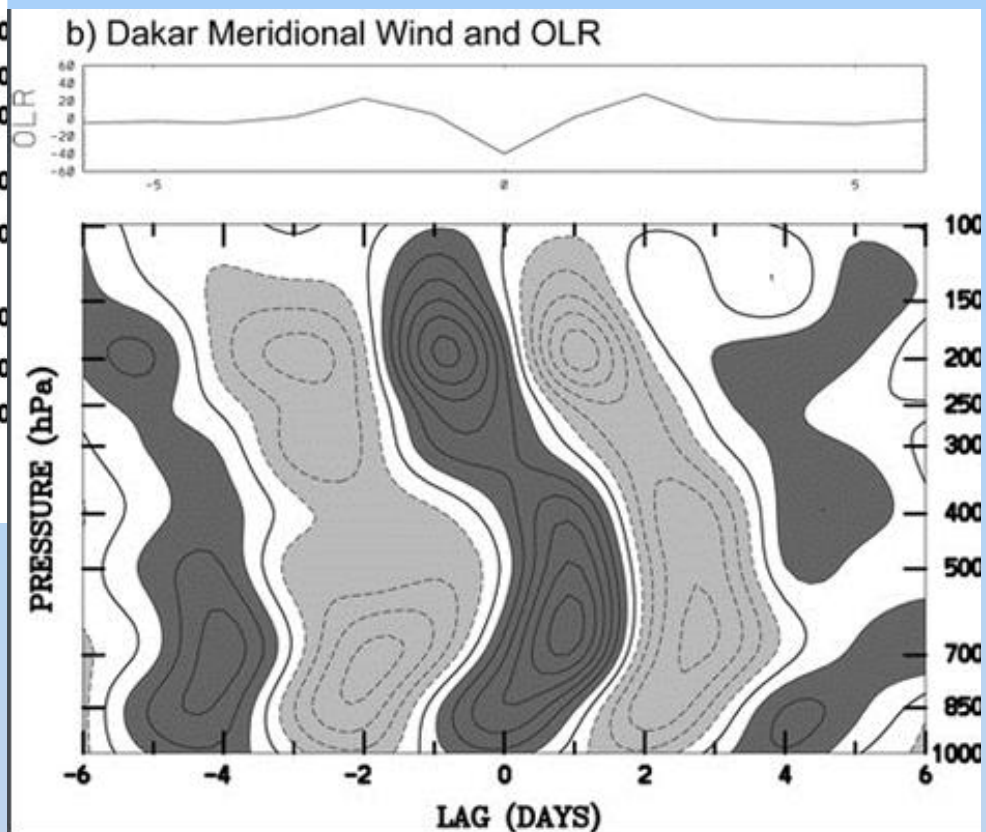


Figure 2.4: Time-height cross-section of the meridional wind anomaly at (a) Bamako and (b) Dakar, scaled to a -40 W m^{-2} perturbation in tropical depression-filtered OLR at the nearest grid point to each station. Contour interval is 0.5 m s^{-1} , negative contours dashed.



Dark (light) shading denotes anomalies greater than (less than) 0.5 m s^{-1} . The associated OLR anomaly is shown at the top in W m^{-2} .
Figure 10 from Kiladis et al. (2006)

Meteorology of Tropical West Africa: The Forecasters' Handbook

Chapter 2: Synoptic Systems - Lead Authors: R Cornforth, Z Mumba, DJ Parker

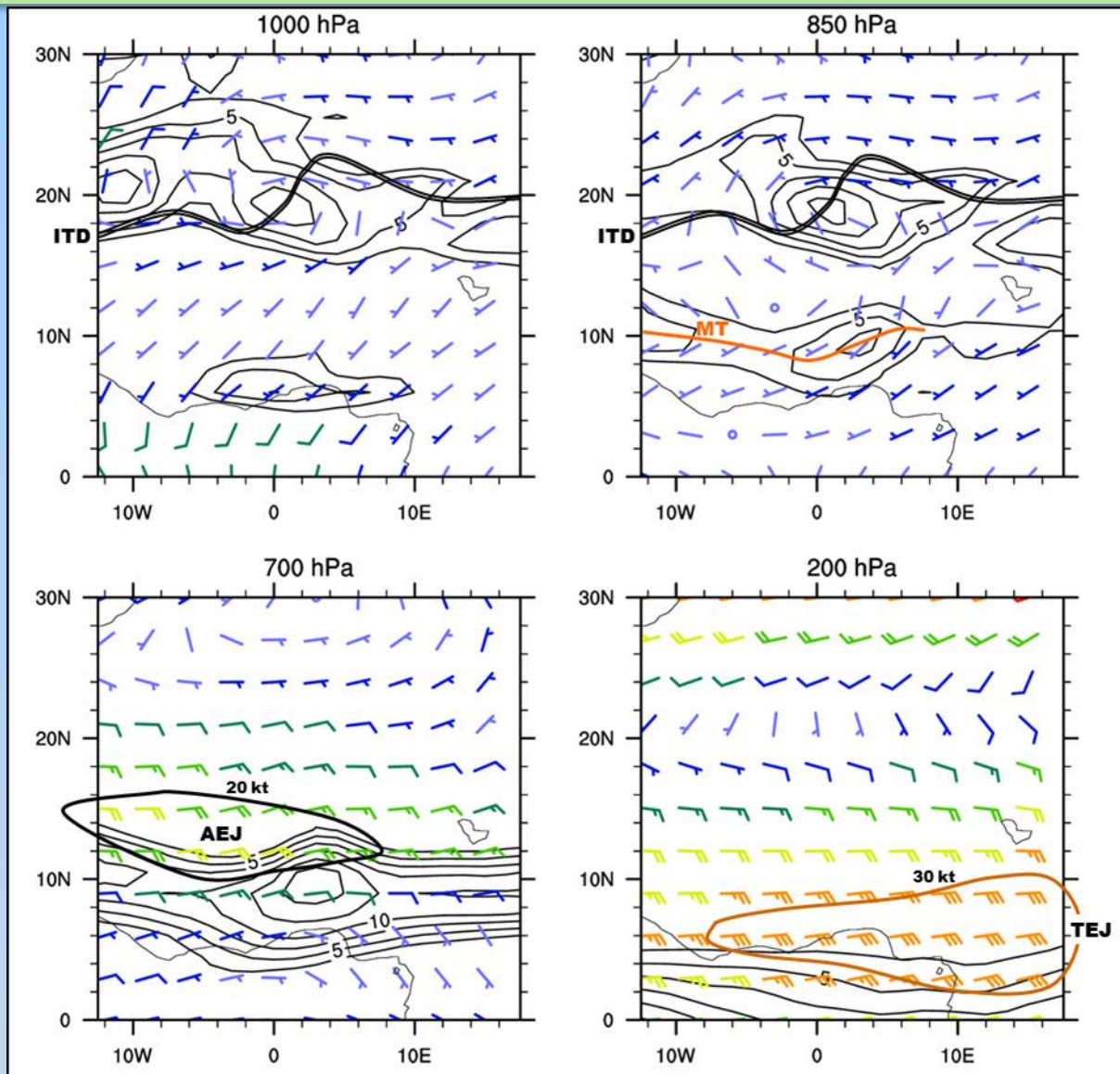


Figure 2.5: Vertical structure of AEW vorticity and winds, from on a composite of AEW cases, based upon the 700 hPa trough axis passing the longitude of Niamey (2.5°E), and comprising 803 cases between 1989 and 2008, identified by the objective identification method of Berry et al. (2007). Composite winds (barbs, coloured in knots) and relative vorticity (positive values greater than $5 \times 10^{-6} \text{ s}^{-1}$ contoured every $5 \times 10^{-6} \text{ s}^{-1}$) are shown on different pressure levels from the ERA-Interim reanalysis dataset.

Meteorology of Tropical West Africa: The Forecasters' Handbook

Chapter 2: *Synoptic Systems* - Lead Authors: R Cornforth, Z Mumba, DJ Parker

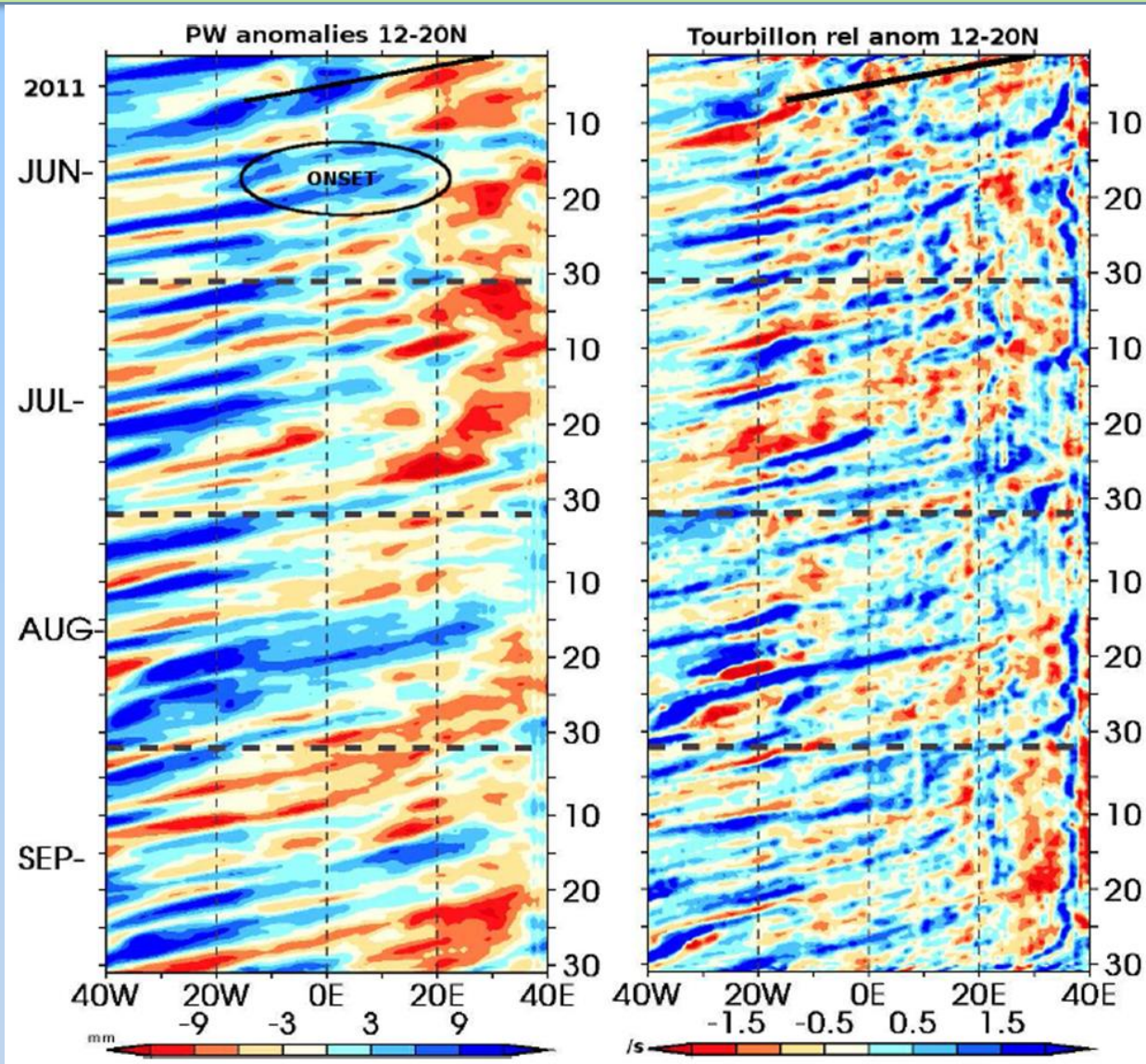


Figure 2.6: Time-longitude diagram of the 2011 June to September intra-seasonal anomalies averaged over the 12°–20°N band: (a) PW (mm) and (b) 850-hPa relative vorticity ($\times 10^{-5} \text{ s}^{-1}$). The black solid lines materialize a slope of a -9 m s^{-1} velocity. From Poan (2013).

Meteorology of Tropical West Africa: The Forecasters' Handbook

Chapter 2: Synoptic Systems - Lead Authors: R Cornforth, Z Mumba, DJ Parker

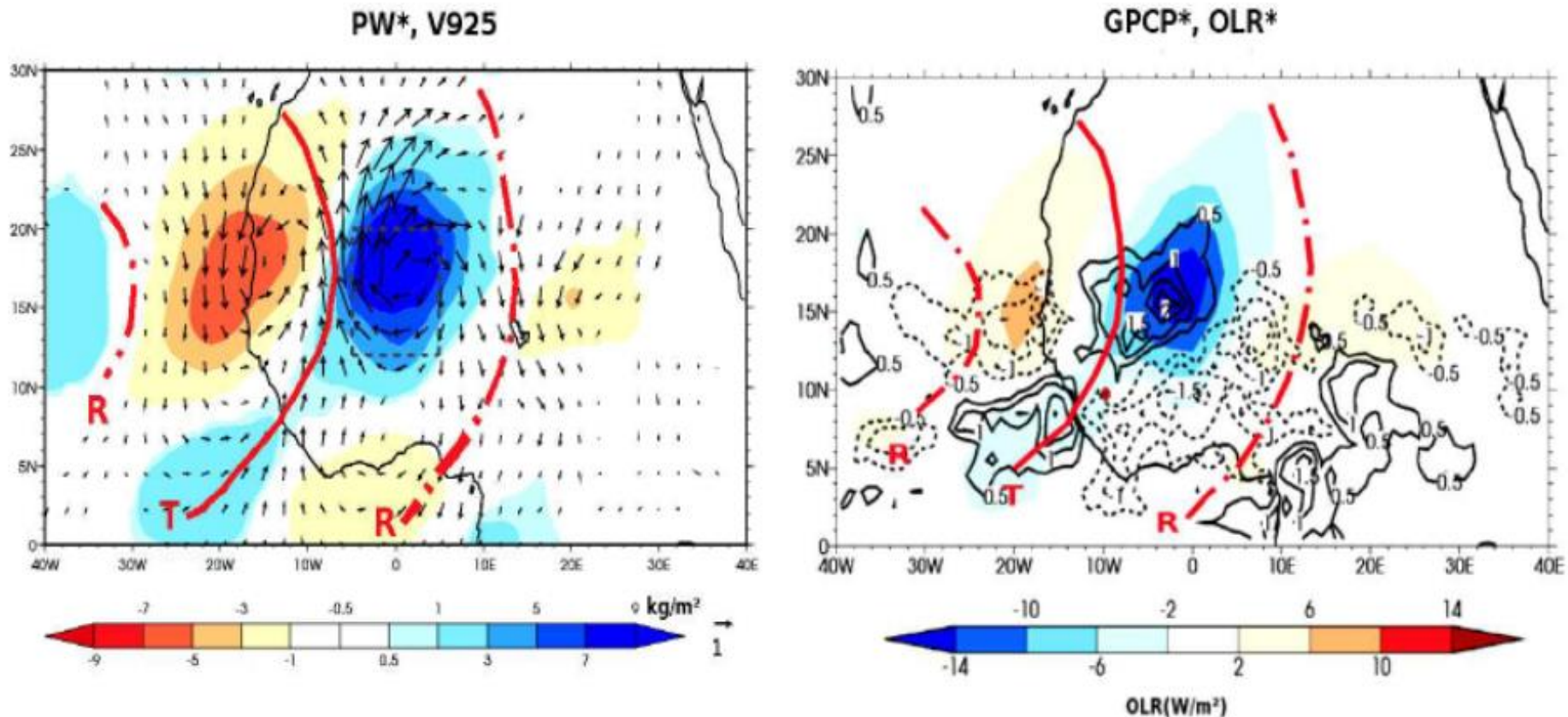


Figure 2.7: Precipitable water anomaly, PW*, 925 hPa winds (left) and GPCP and OLR anomaly fields (right), based on a composite on the PW* field of AEWs (Poan et al., 2013). The (red) trough and ridge lines are based on the wind fields at 600 hPa. Note that the relationship of OLR with the wave structure must be treated with caution because these structures do not effectively capture the very intense squall lines which propagate to the west of the AEW trough into areas of lower PW*.

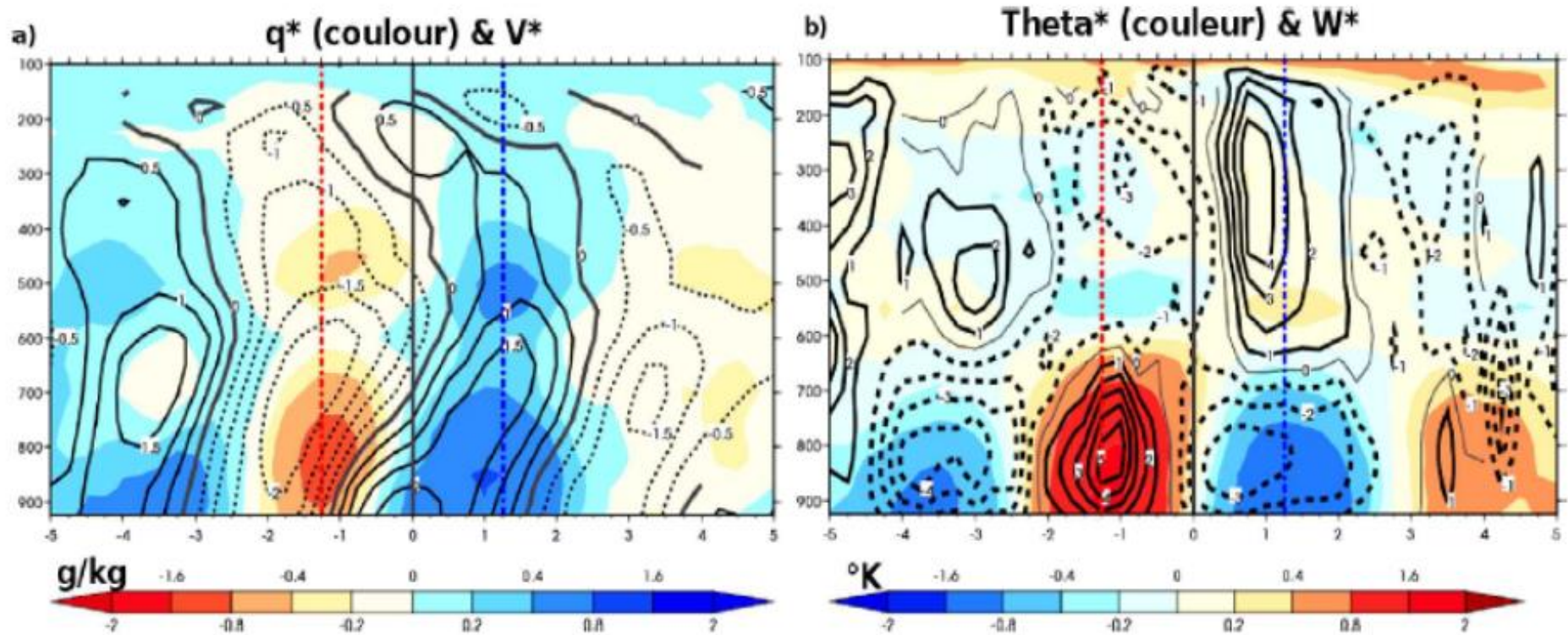


Figure 2.8 Vertical-lag composite of (a) specific humidity (g kg^{-1} , shaded) and meridional wind (m s^{-1} , contours) anomalies, (b) potential temperature (K, shaded) and vertical wind (mm s^{-1} , contours) anomalies, based on a composite on the PW^* field of AEWs. The vertical black line corresponds to the trough location at t_0 , whereas vertical dashed red and blue lines correspond to the passage of the dry/warm and moist/cold stages respectively (at $t_0 - 1.25$ and $t_0 + 1.25$). From Poan (2013).

Meteorology of Tropical West Africa: The Forecasters' Handbook

Chapter 2: Synoptic Systems - Lead Authors: R Cornforth, Z Mumba, DJ Parker

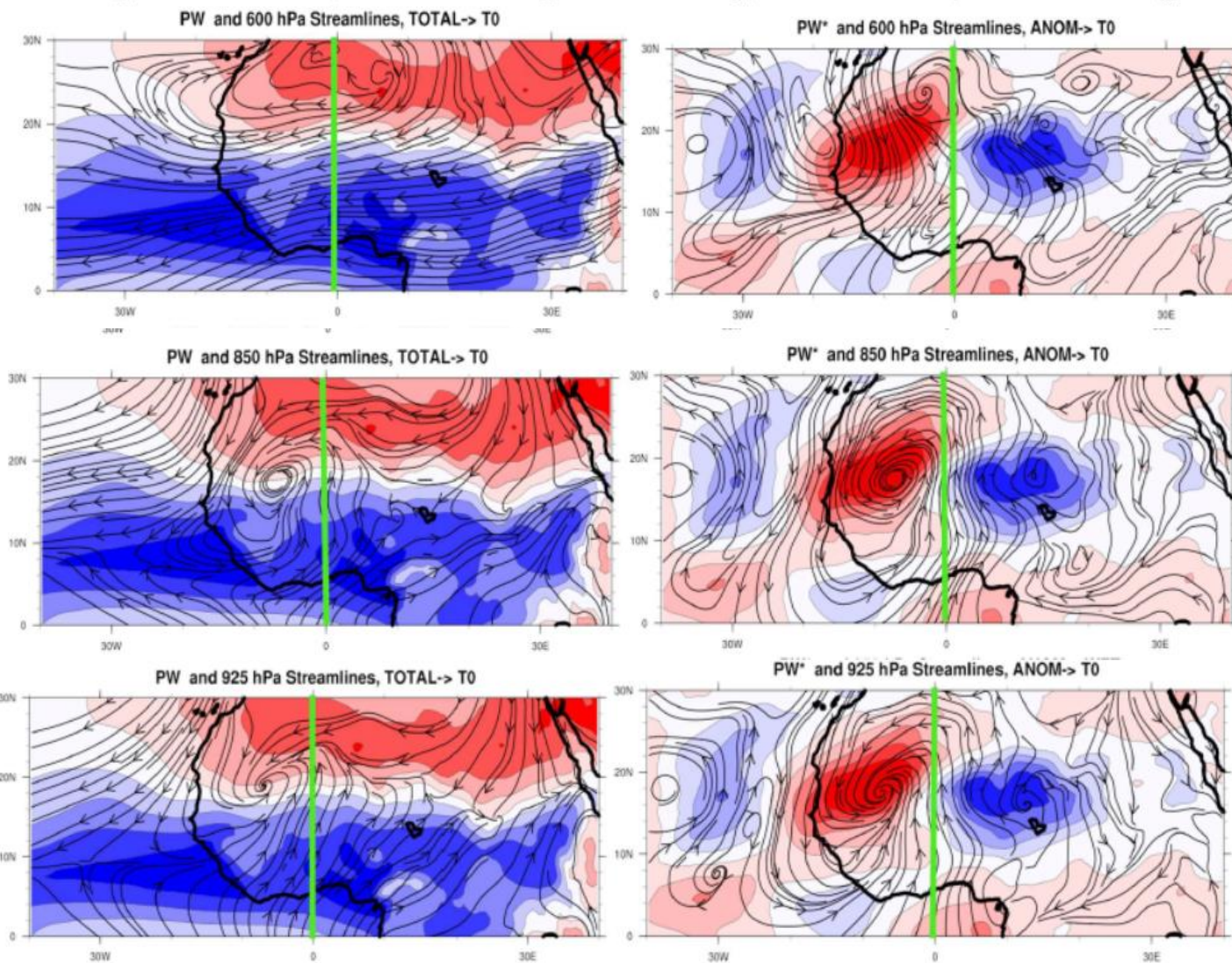


Figure 2.9: Composites of streamlines and PW (mm, shaded) fields at 925, 850 and 600 hPa at the passage (t0) of the AEW at 0°E. The left and right columns correspond to the full and anomaly fields respectively. From Poan (2013).

Meteorology of Tropical West Africa: The Forecasters' Handbook

Chapter 2: Synoptic Systems - Lead Authors: R Cornforth, Z Mumba, DJ Parker

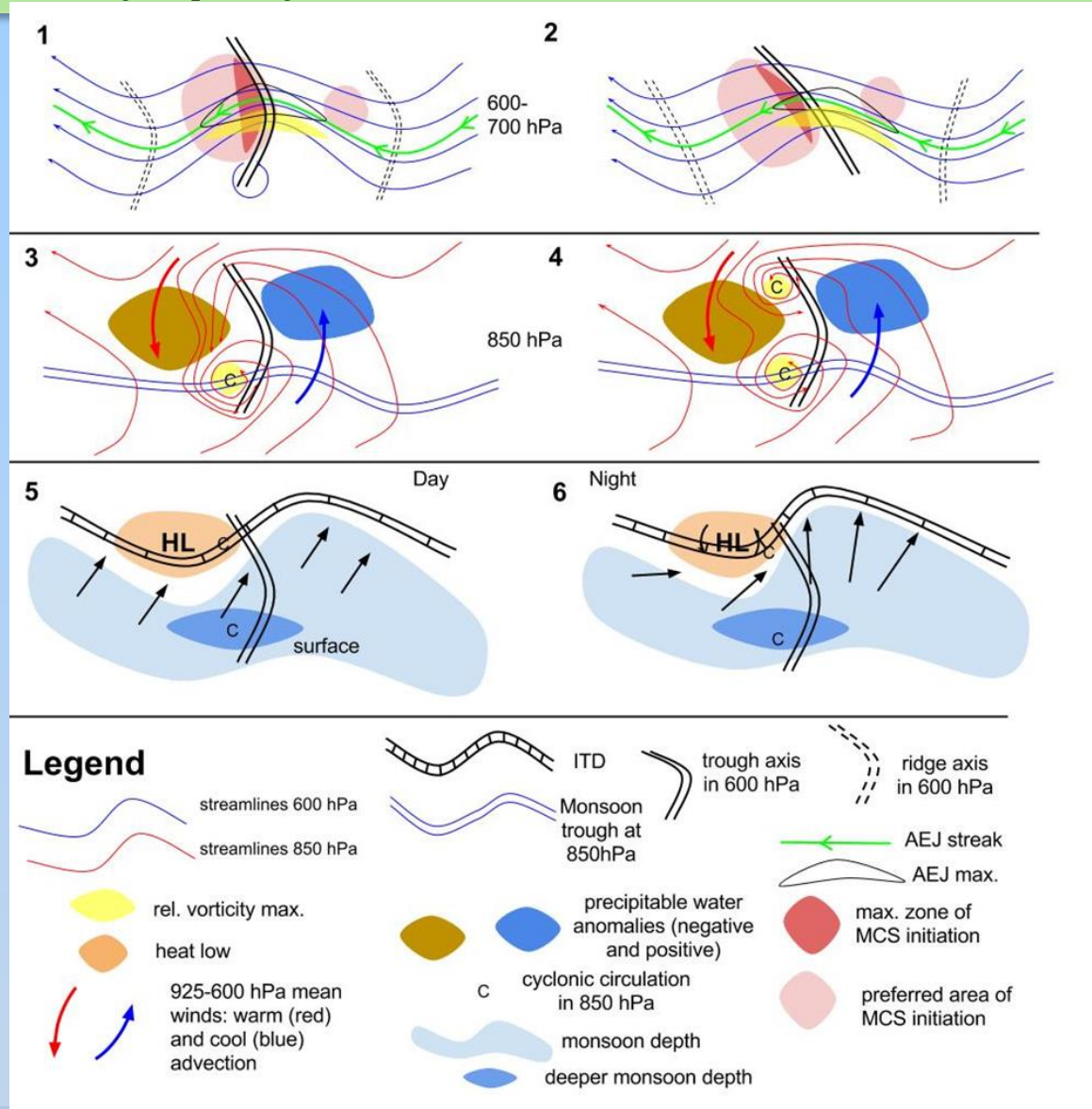


Figure 2.10: Schematic of the various observable elements of an AEW, and likely relationships between these. Left hand panels show a “normal” situation, as far as this exists, while right hand panels show common alternatives. For example, the structure in panel 2 would be expected in an environment with additional barotropic shear, with a stronger easterly wind to the north (i.e. $U_y < 0$).

Meteorology of Tropical West Africa: The Forecasters' Handbook

Chapter 2: *Synoptic Systems* - Lead Authors: R Cornforth, Z Mumba, DJ Parker

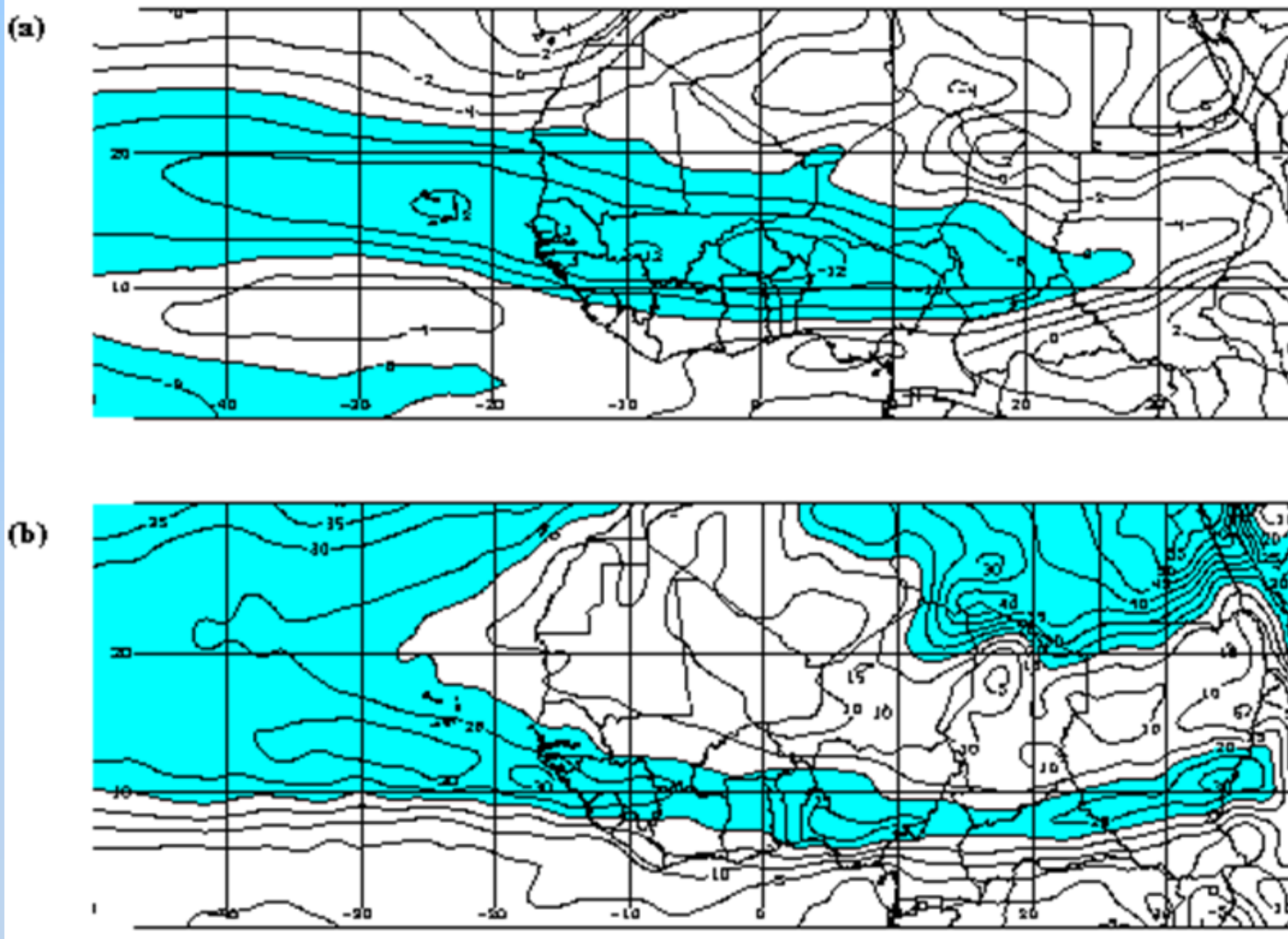


Figure 2.11: Illustration of the meridional potential vorticity (PV) reversal. Panels (a) and (b) (based on operational ECMWF analyses and adapted from Figure 1 in Thorncroft et al. (2003)) show (a) zonal wind and (b) PV, on the 600 hPa surface. The maximum PV on this level is to the south of the AEJ maximum (each shaded blue), with low PV to the north of the AEJ.

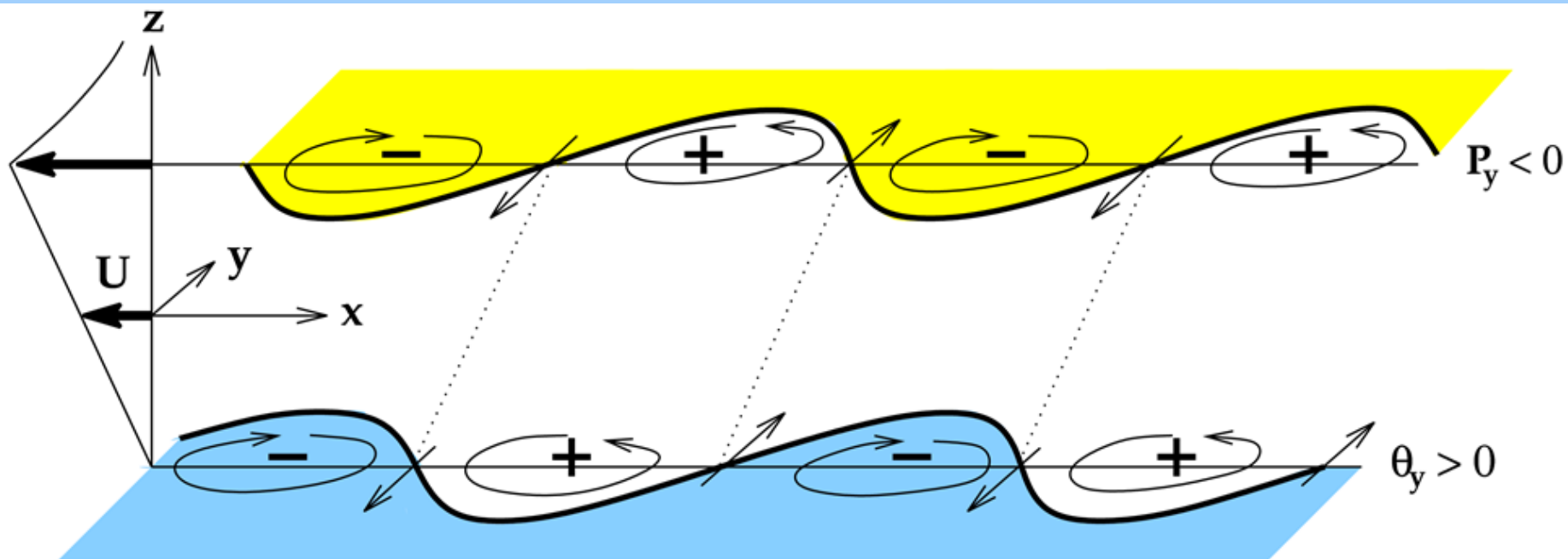
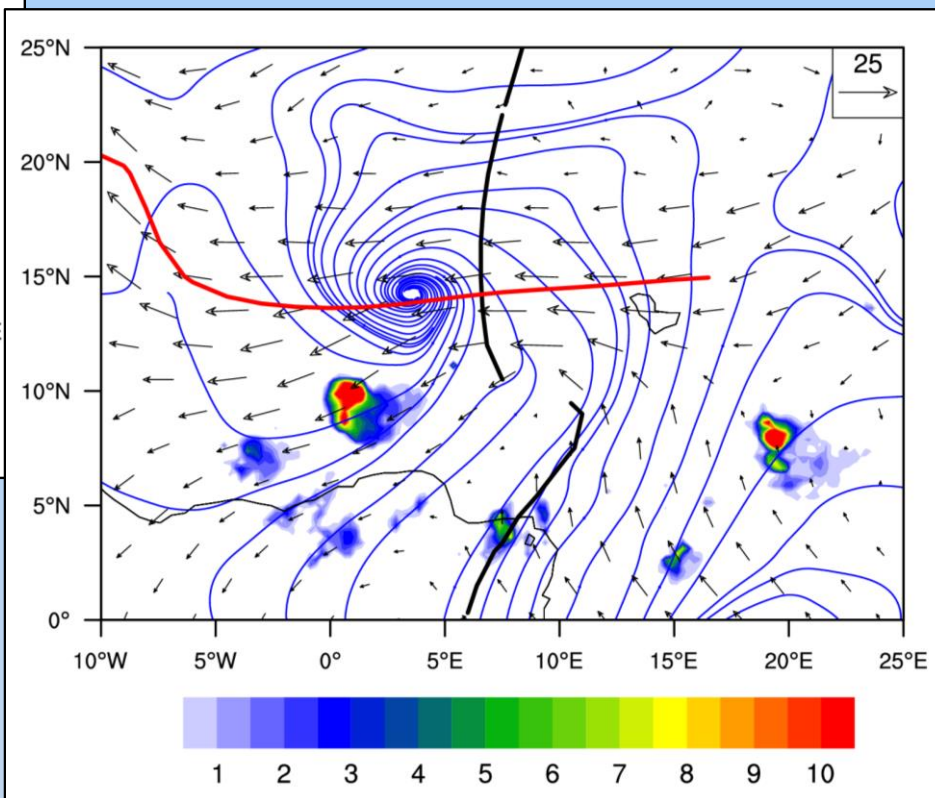
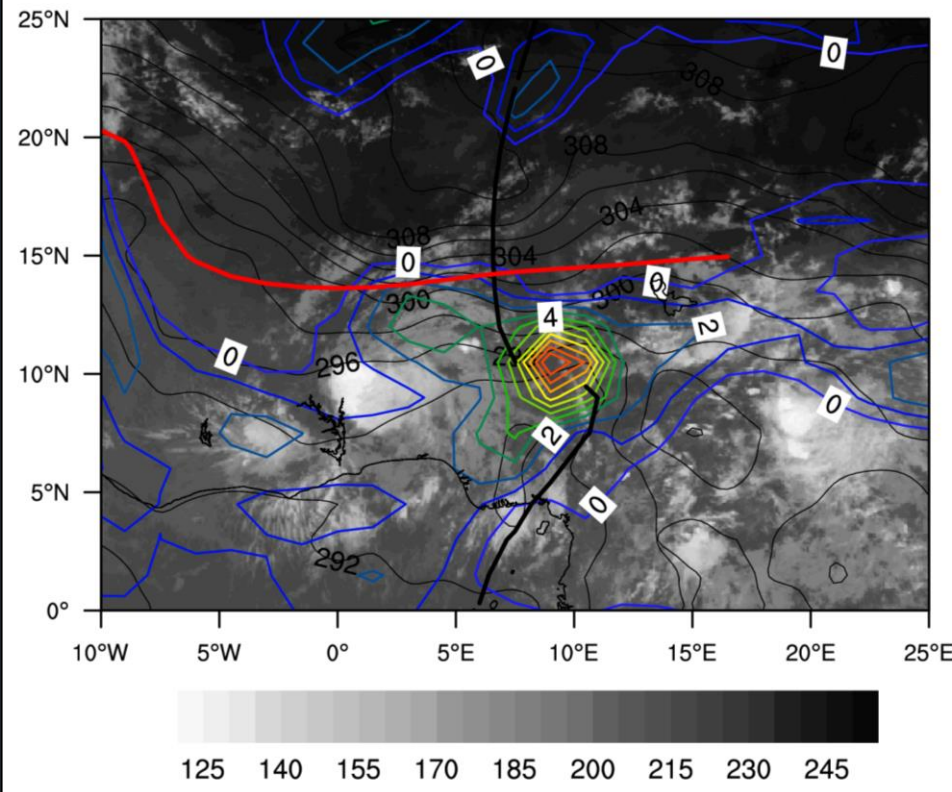


Figure 2.12: A schematic depicting the meridional displacements of air and associated circulations within an African Easterly Wave that are predicted for a “baroclinic” growth configuration. An “upper Rossby wave component” propagates along the African Easterly Jet and interacts with a “lower wave” propagating westwards.

Meteorology of Tropical West Africa: The Forecasters' Handbook

Chapter 2: Synoptic Systems - Lead Authors: R Cornforth, Z Mumba, DJ Parker

Figure 2.13: Synoptic maps of ECMWF ERA-Interim reanalysis fields on 1st August 2000, 1200 UTC: (a, LEFT) 700 hPa relative vorticity (coloured lines), 925hPa temperature (thin black lines), 700 hPa objective trough (thick black line) and objective jet axes (thick red line, see Berry et al. (2007) for definition).



(b, RIGHT) Mean TRMM 3B42 estimated precipitation rate (mm hr-1, shaded according to legend), Streamlines at 925 hPa (blue streamlines) and wind vectors at 700 hPa. The same objective trough and jet axes as in (a) are overlaid.

Meteorology of Tropical West Africa: The Forecasters' Handbook

Chapter 2: *Synoptic Systems* - Lead Authors: R Cornforth, Z Mumba, DJ Parker

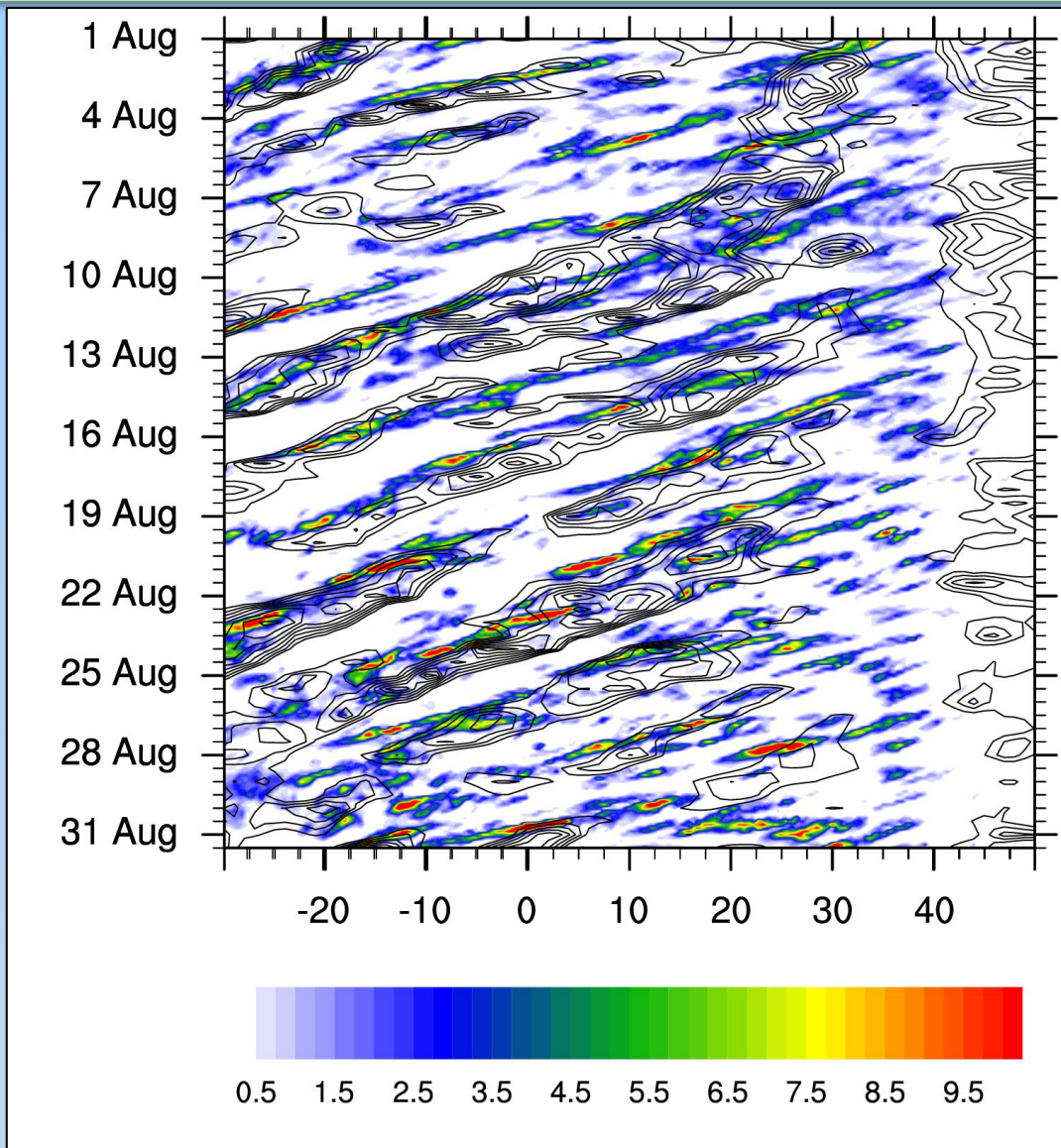


Figure 2.14: Hovmoller space-time diagram of 700 hPa curvature vorticity (positive values greater than $2 \times 10^{-6} \text{ s}^{-1}$ contoured every $2 \times 10^{-6} \text{ s}^{-1}$) from GFS operational analyses and CMORPH precipitation estimate (shaded in mm hr⁻¹, according to colour bar), both averaged 5-15°N for the month of August 2004.

Meteorology of Tropical West Africa: The Forecasters' Handbook

Chapter 2: Synoptic Systems - Lead Authors: R Cornforth, Z Mumba, DJ Parker

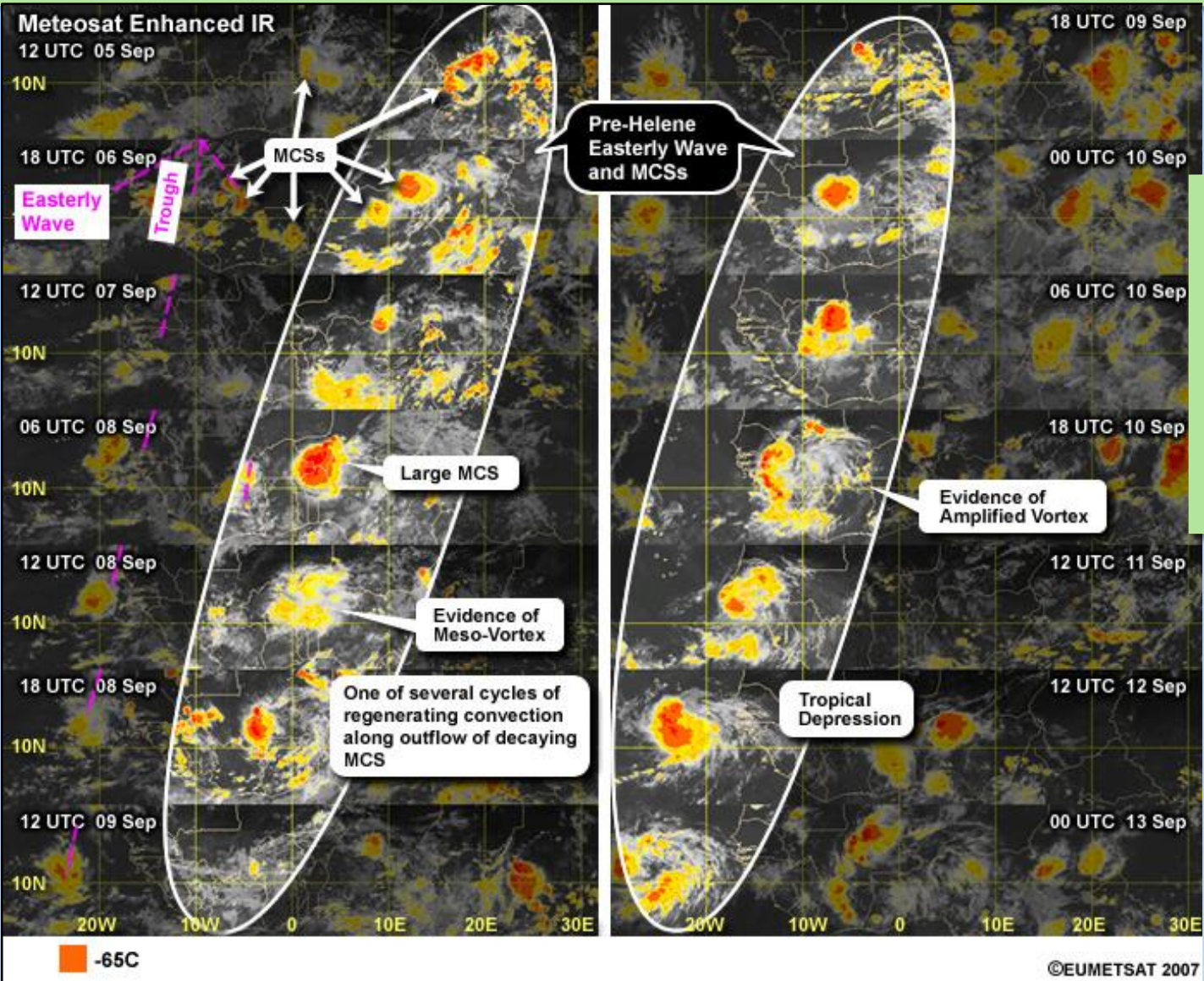


Figure 2.15: Enhanced IR images of African Easterly waves and MCSs between 1200 UTC 5 September and 0000 UTC 13 September 2006, precursors to Helene (2006). From Laing and Evans, 2015

Meteorology of Tropical West Africa: The Forecasters' Handbook

Chapter 2: Synoptic Systems - Lead Authors: R Cornforth, Z Mumba, DJ Parker

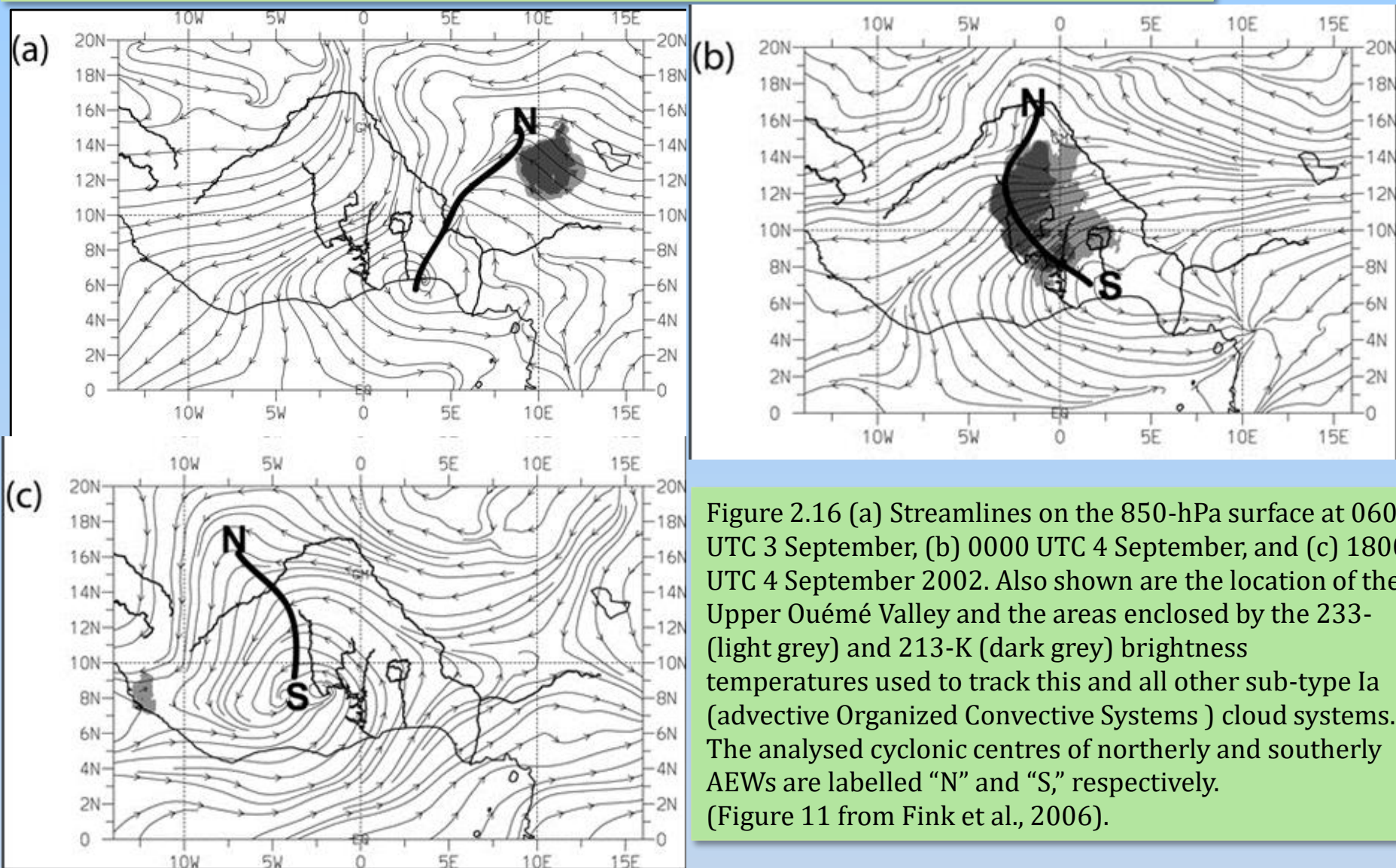


Figure 2.16 (a) Streamlines on the 850-hPa surface at 0600 UTC 3 September, (b) 0000 UTC 4 September, and (c) 1800 UTC 4 September 2002. Also shown are the location of the Upper Ouémé Valley and the areas enclosed by the 233- (light grey) and 213-K (dark grey) brightness temperatures used to track this and all other sub-type Ia (advective Organized Convective Systems) cloud systems. The analysed cyclonic centres of northerly and southerly AEWs are labelled "N" and "S," respectively. (Figure 11 from Fink et al., 2006).

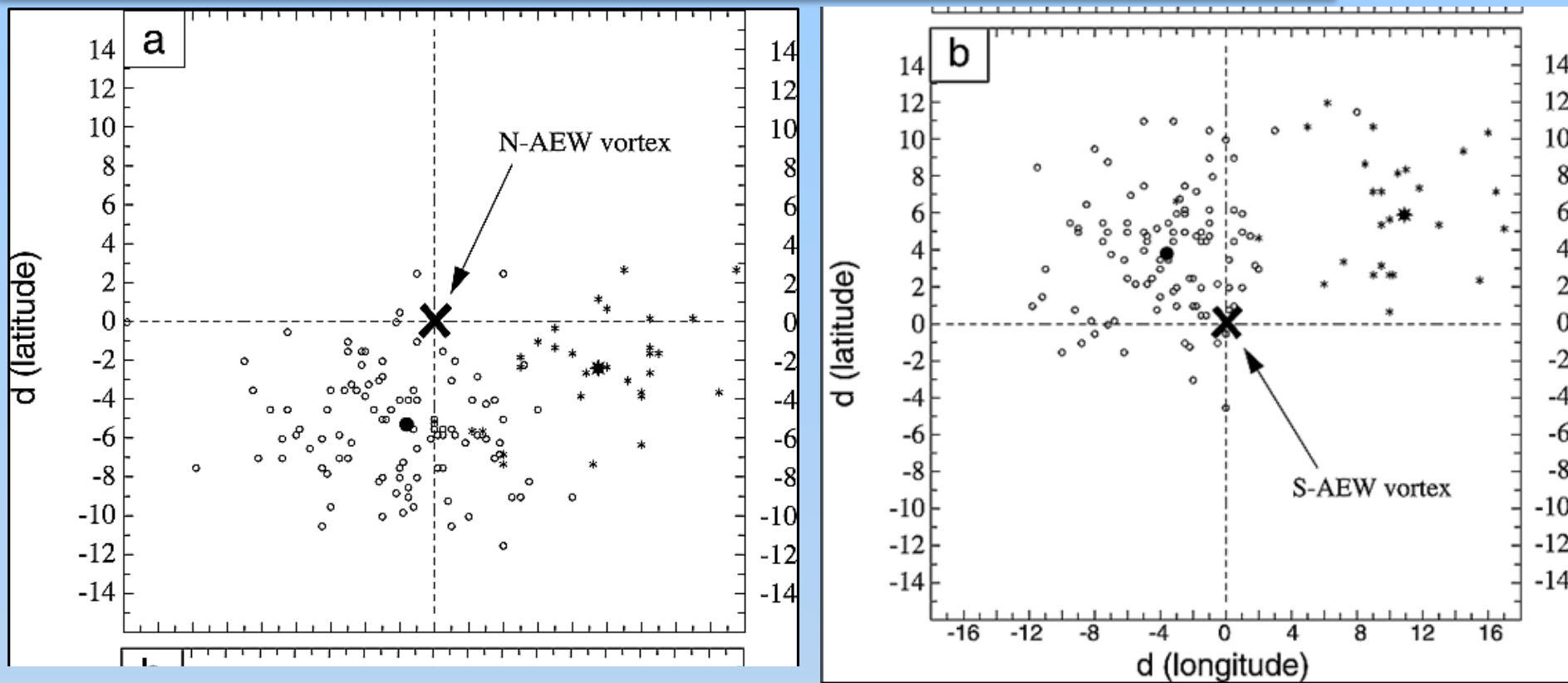


Figure 2.17: Scatterplots of the positions of origin points of Squall Lines relative to the simultaneous locations of the accompanying (a) northerly and (b) southerly AEW vortices. The abscissa (ordinate) denotes the longitudinal (latitudinal) distance with negative values indicating that the Squall Line origin is west (south) of the respective vortices. (Figure 11 from Fink and Reiner, 2003).

(a) October to March

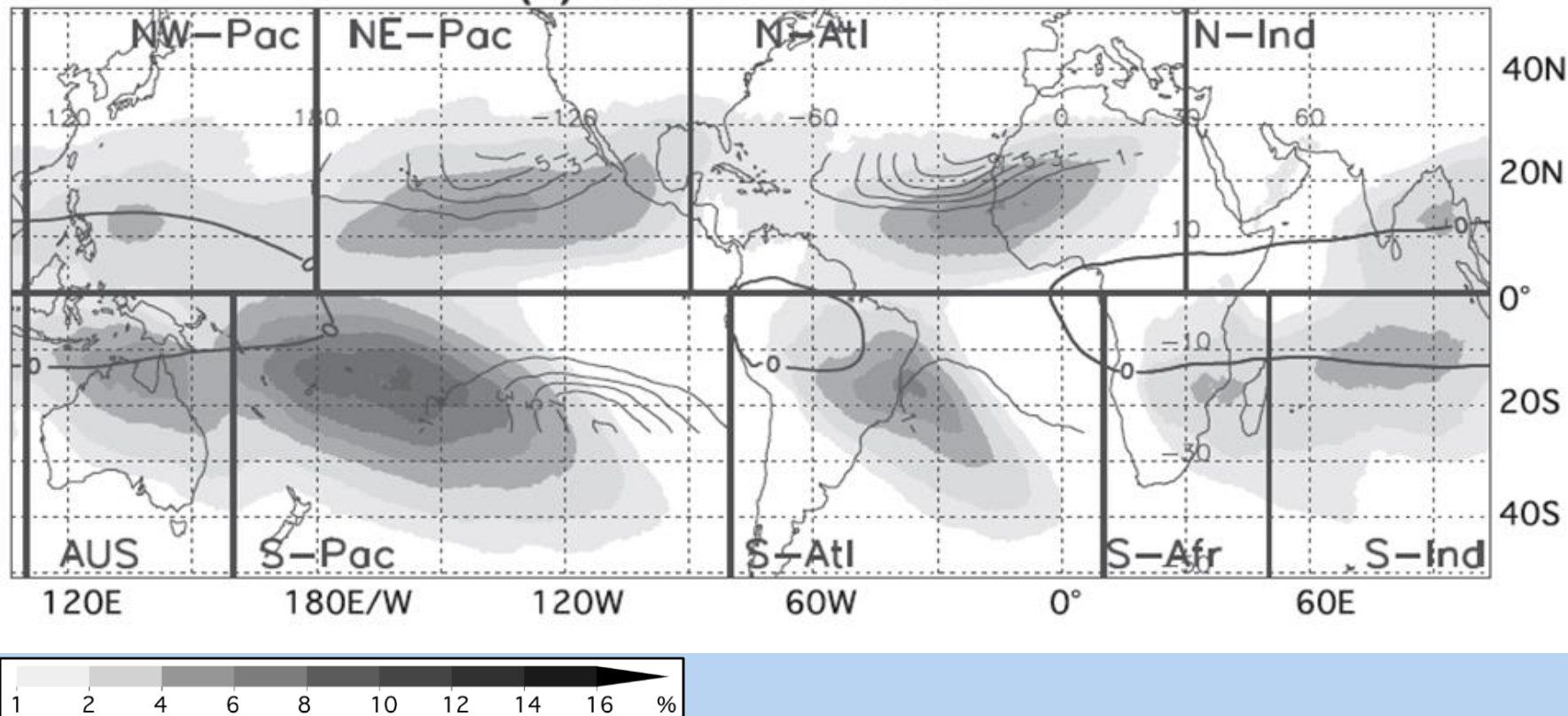


Figure 2.18 Mean Tropical Plume frequency (%; shaded) for Oct–Mar between 1983/84 and 2005/06. The contours display the mean frequency of troughs at low latitudes (%) detected by Fröhlich and Knippertz (2008) in the ERA-40 data between 1980 and 2001. The bold grey contour presents the zero line of the mean zonal wind at 200 hPa indicating equatorial easterlies from the western Pacific to the eastern Atlantic and over South America, with westerlies elsewhere. (Figure 4a from Fröhlich et al., 2013.)

Meteorology of Tropical West Africa: The Forecasters' Handbook

Chapter 2: *Synoptic Systems* - Lead Authors: R Cornforth, Z Mumba, DJ Parker

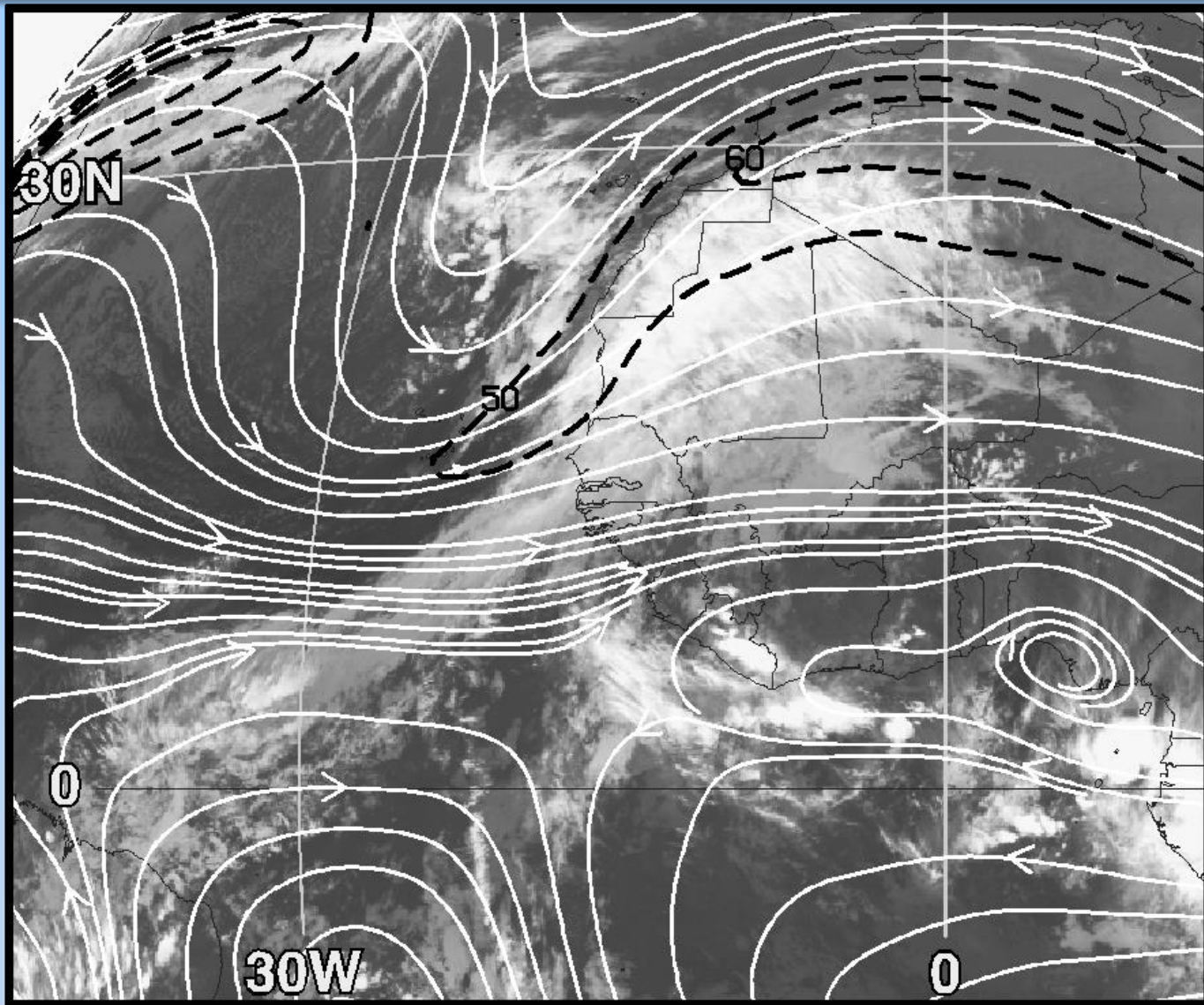


Figure 2.19 Meteosat infrared satellite image for 0000 UTC 10 January 2002 with superimposed isotachs (dashed black in m s^{-1}) and streamlines (in white), both at the 345 K isentropic level. (slightly modified version of Fig 2c from Knippertz and Martin, 2005.)

Meteorology of Tropical West Africa: The Forecasters' Handbook

Chapter 2: Synoptic Systems - Lead Authors: R Cornforth, Z Mumba, DJ Parker

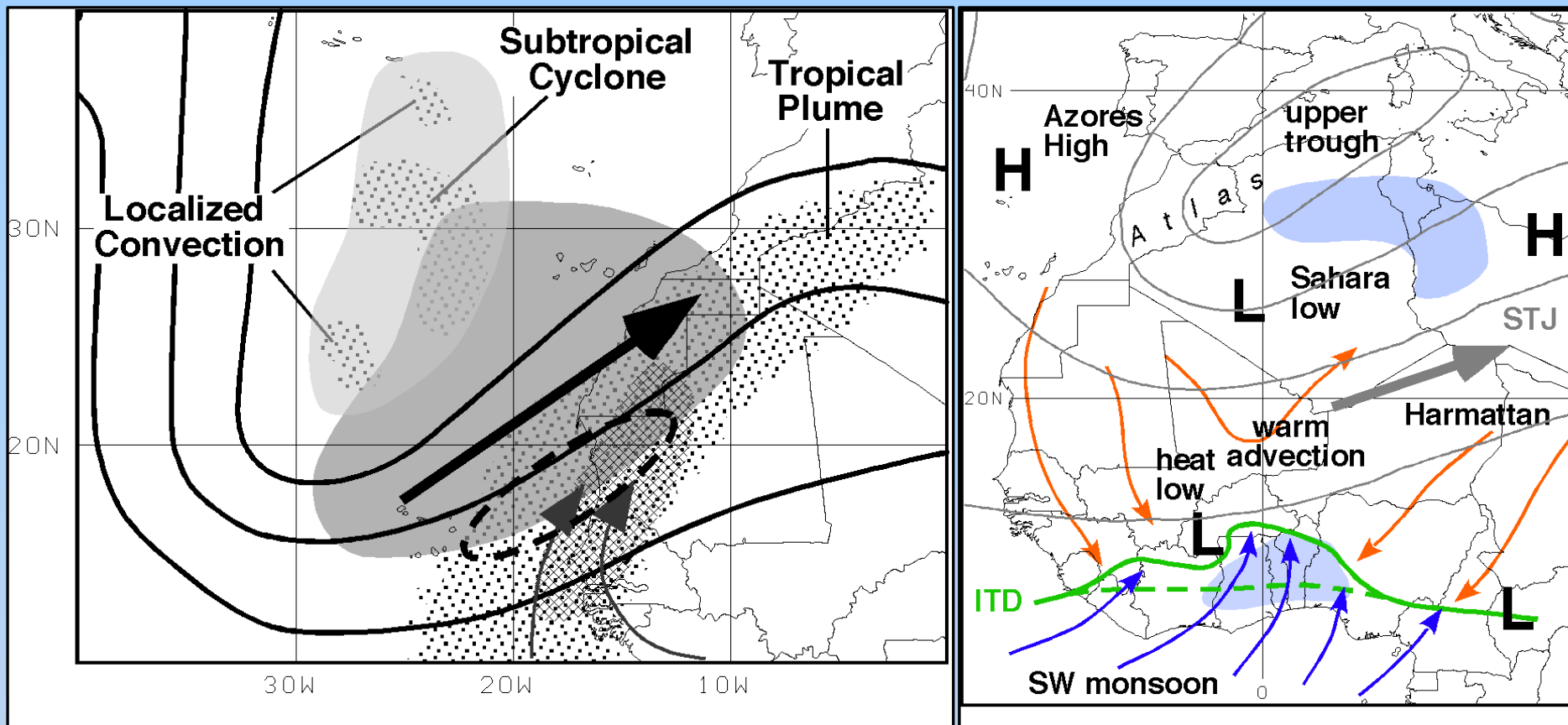
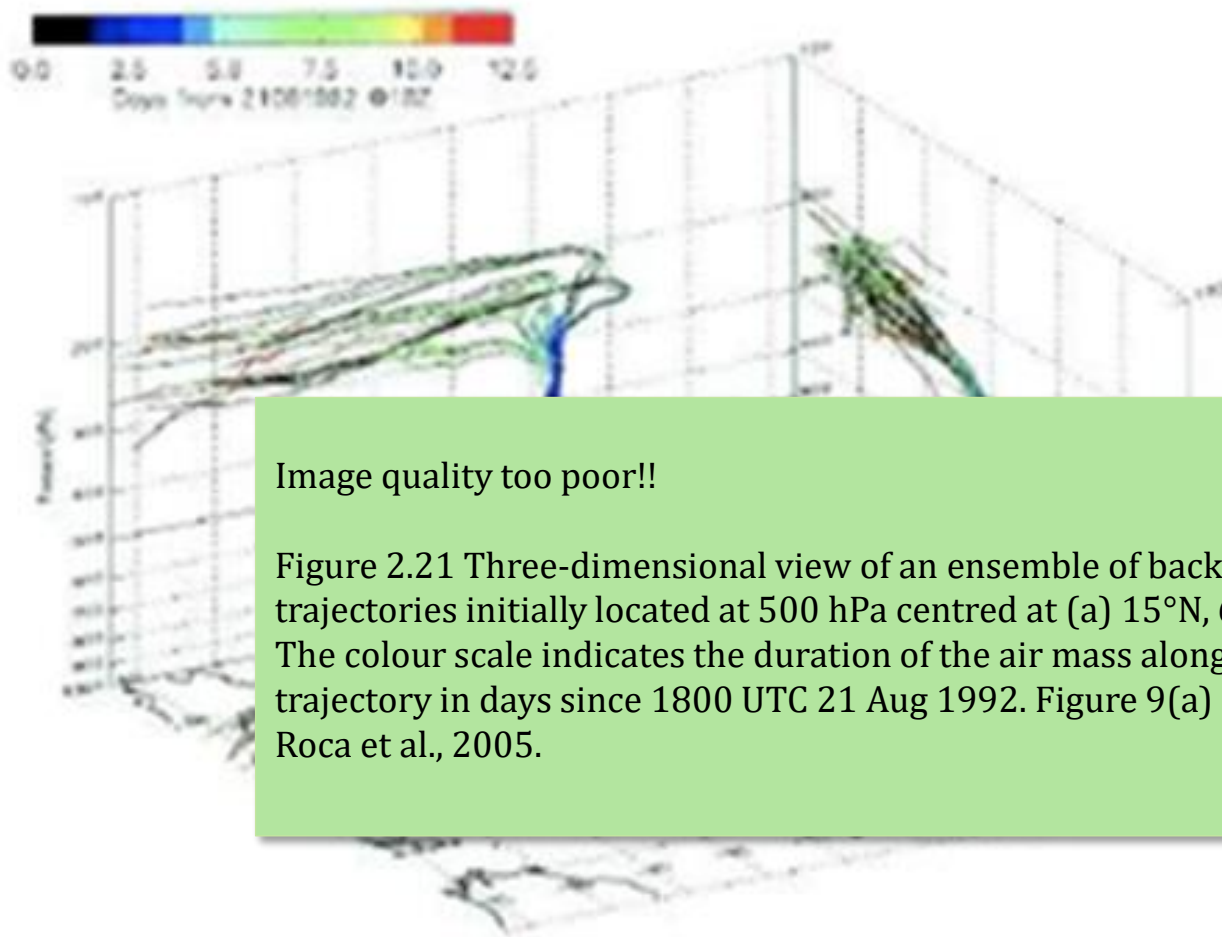


Figure 2.20: Schematic depictions of the large-scale circulation associated with dry-season precipitation over West Africa associated with low-latitude upper-level disturbances from the extratropics. Left panel: Cases with a direct influence from the upper-trough, mostly affecting the western Sahel. Figure 11 from Knippertz, 2007. Right panel: Cases with an indirect influence from the upper-trough, mostly affecting the Soudano-Sahelian zone.



Meteorology of Tropical West Africa: The Forecasters' Handbook

Chapter 2: Synoptic Systems - Lead Authors: R Cornforth, Z Mumba, DJ Parker

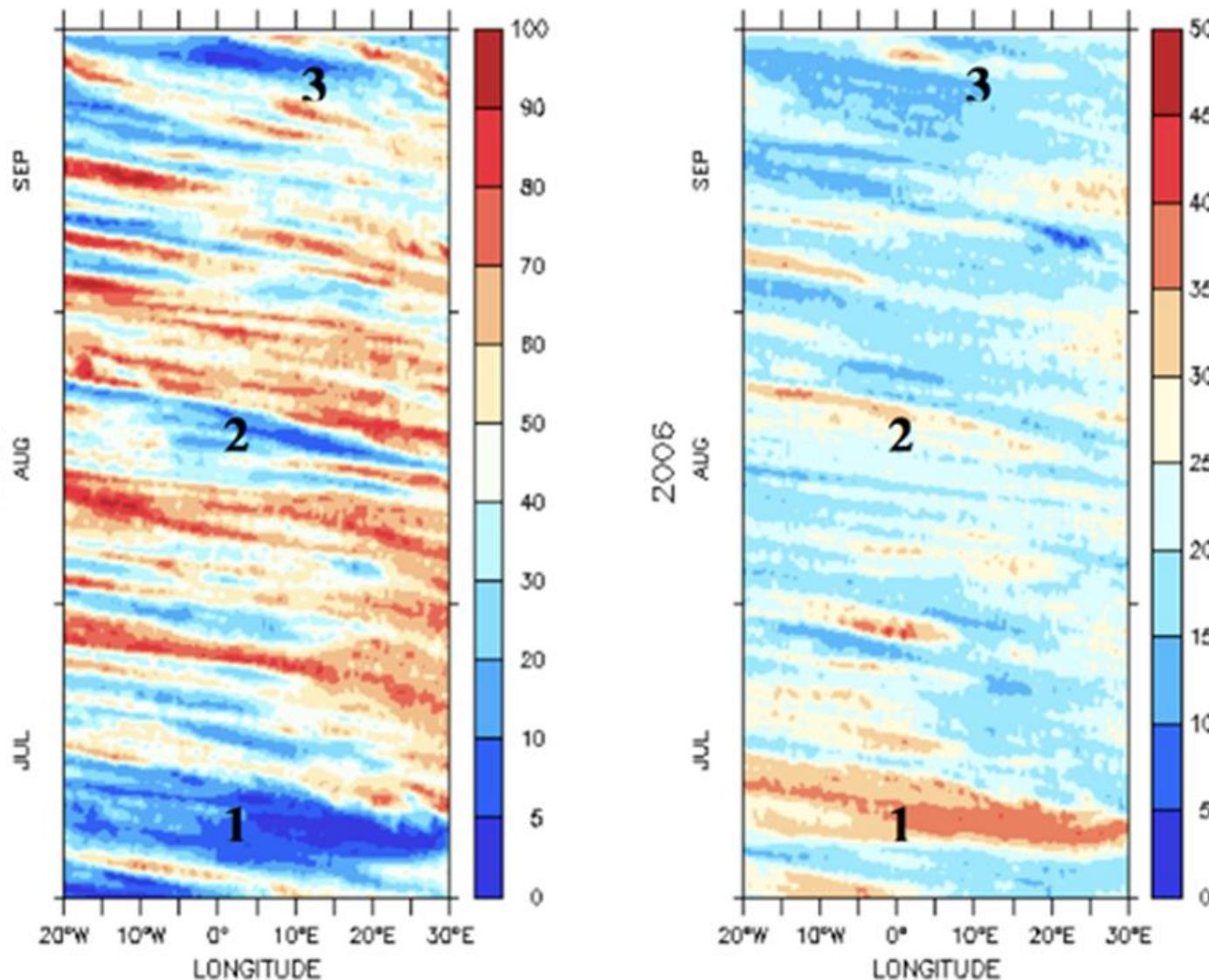
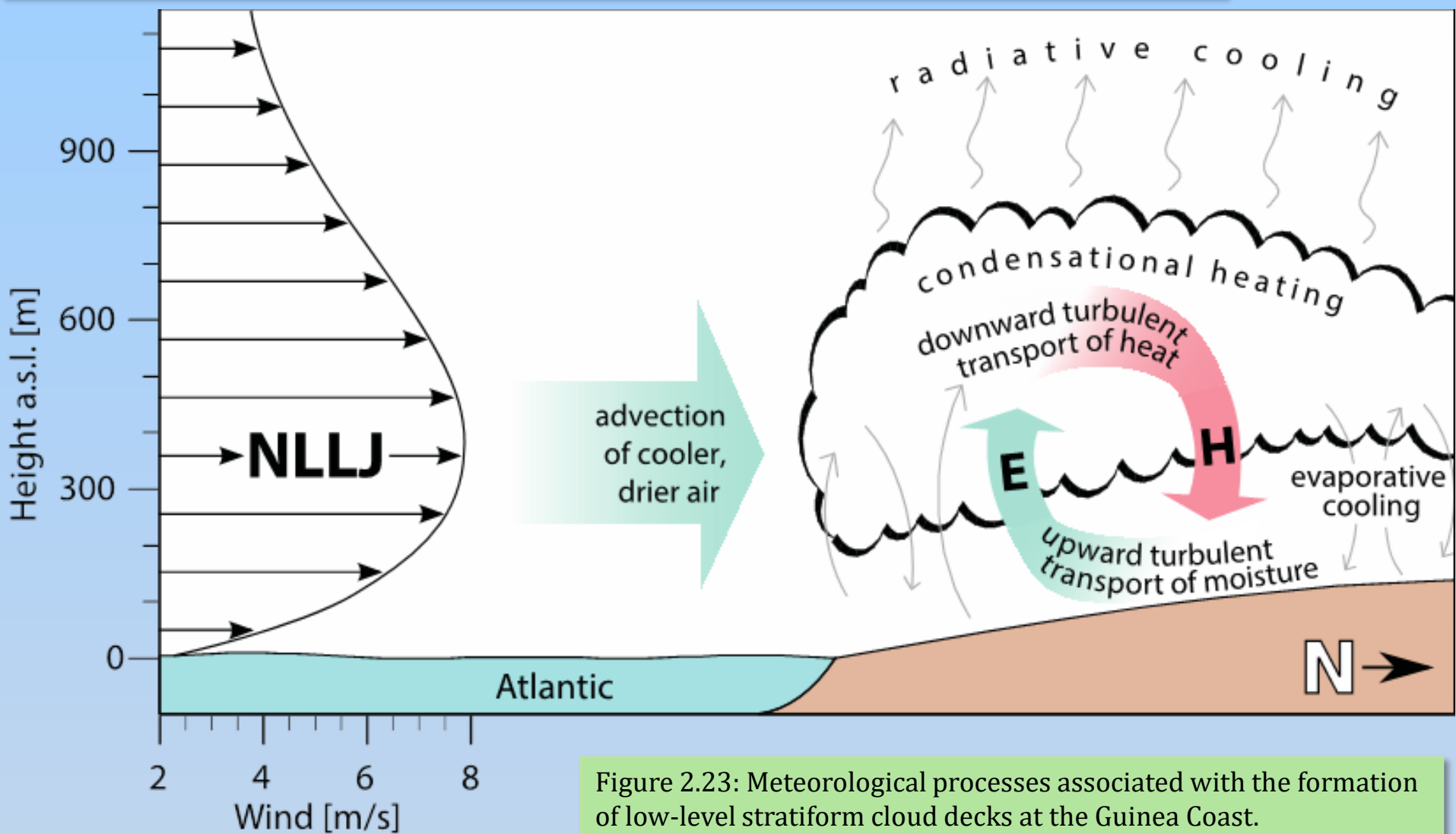


Figure 2.22: Time longitude diagram averaged over the 12.5°N-17.5°N latitude belt for the 2006 season. Left: relative humidity at 500 hPa. Right: latitude of last saturation (degrees North). The bold numbers correspond to the 3 identified large events. Both the humidity and the last saturation information come from a Lagrangian modelling effort (Pierrehumbert, 1998; Pierrehumbert and Roca, 1998) fed by NCEP/GFS analysis.



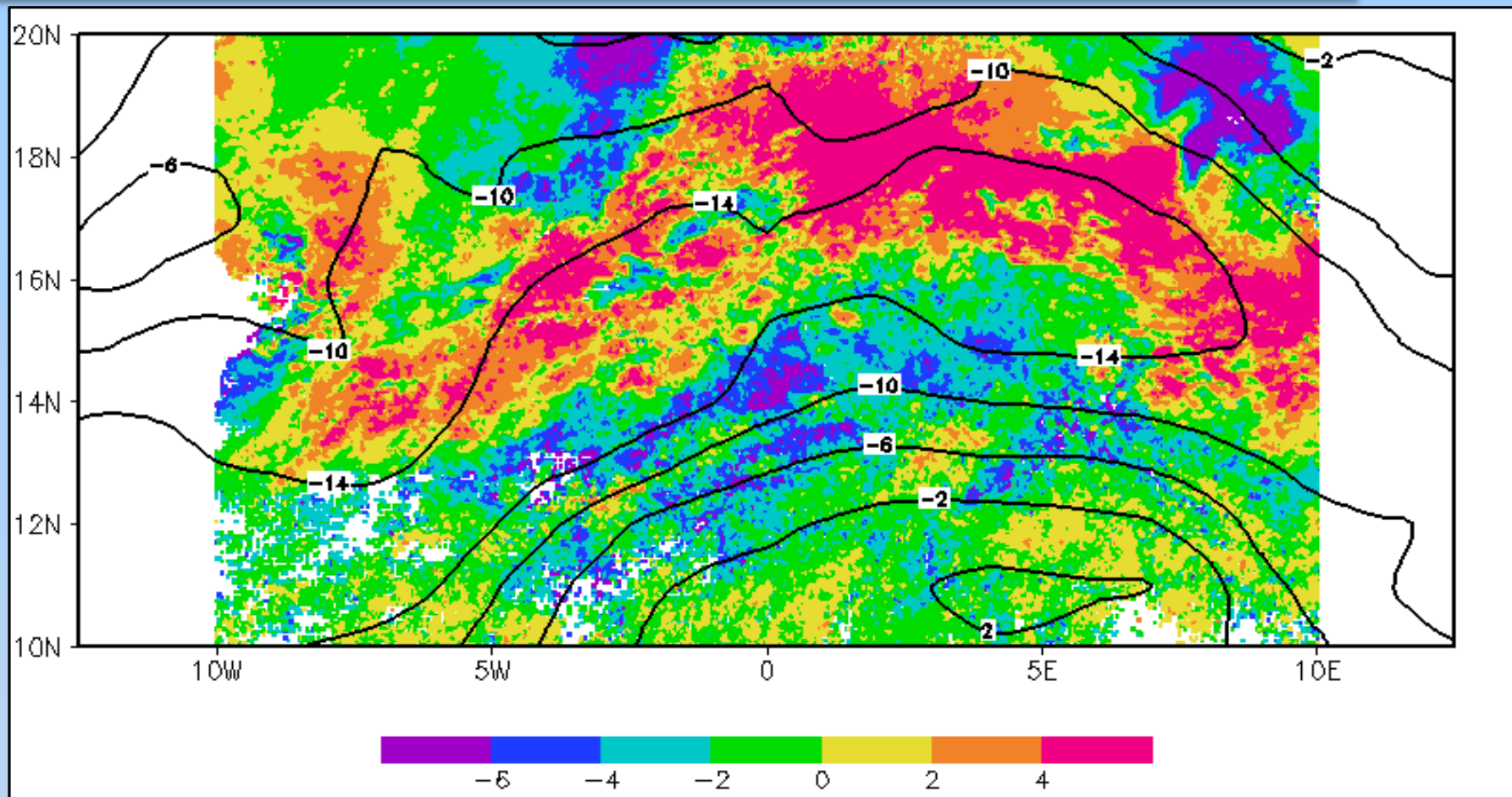


Figure 2.24: Daytime land surface temperatures [shading; K] on 26th July 2006 derived from Meteosat Second Generation (<http://landsaf.meteo.pt/as>) anomalies from the 3-week mean. The (pink) band of positive temperature anomalies denotes a dry region whilst the relatively cool (blue) conditions to the south indicate high soil moisture from storms in the previous 36 hours.

Meteorology of Tropical West Africa: The Forecasters' Handbook

Chapter 2: *Synoptic Systems* - Lead Authors: R Cornforth, Z Mumba, DJ Parker

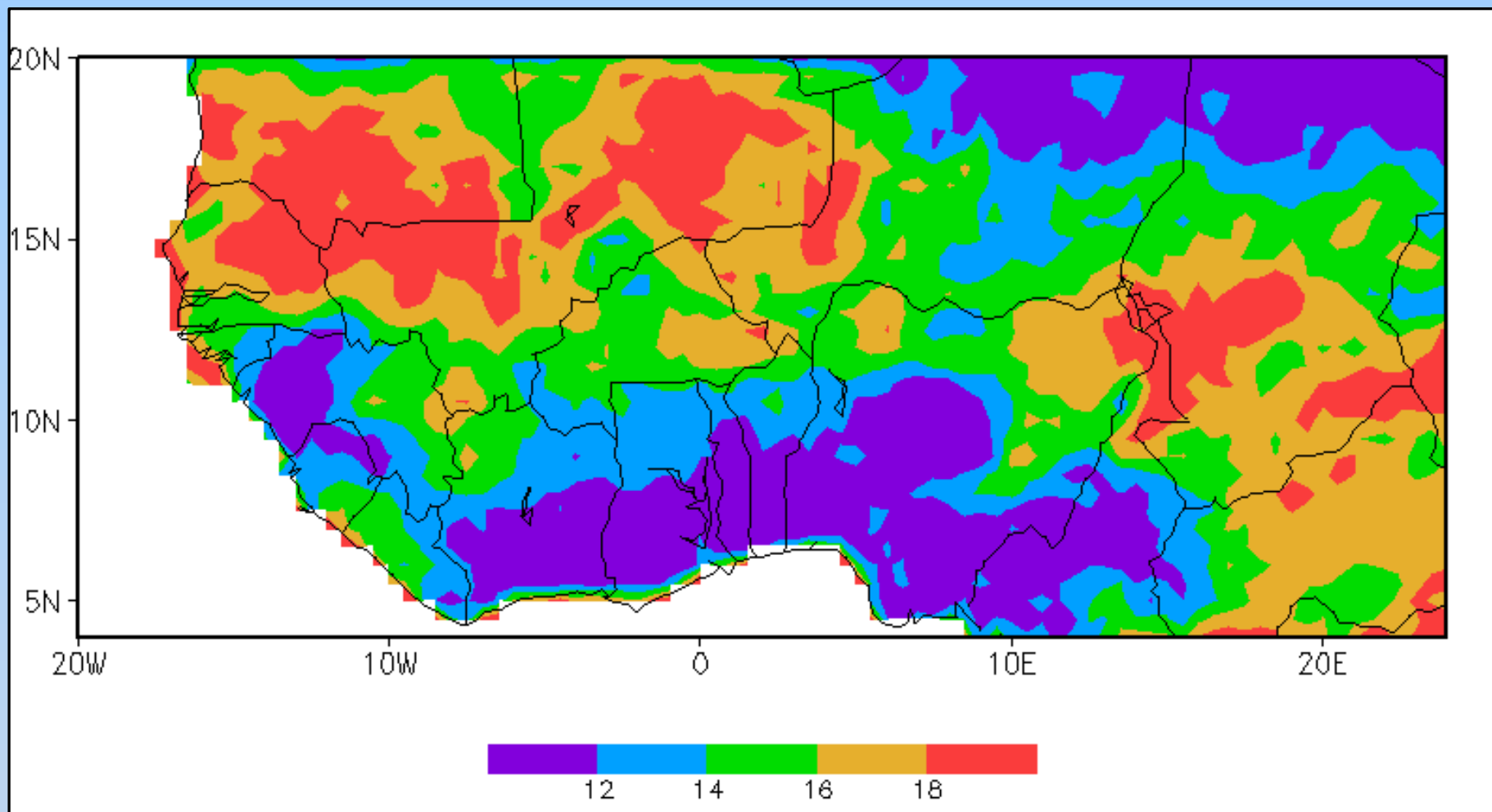


Figure 2.25: Standard deviation of sensible heat flux H [Wm^{-2}] averaged over July-September 2004-2007 from the ALMIP model ensemble (Boone et al., 2009). The daily data have been filtered to remove variability with periods exceeding 10 days.

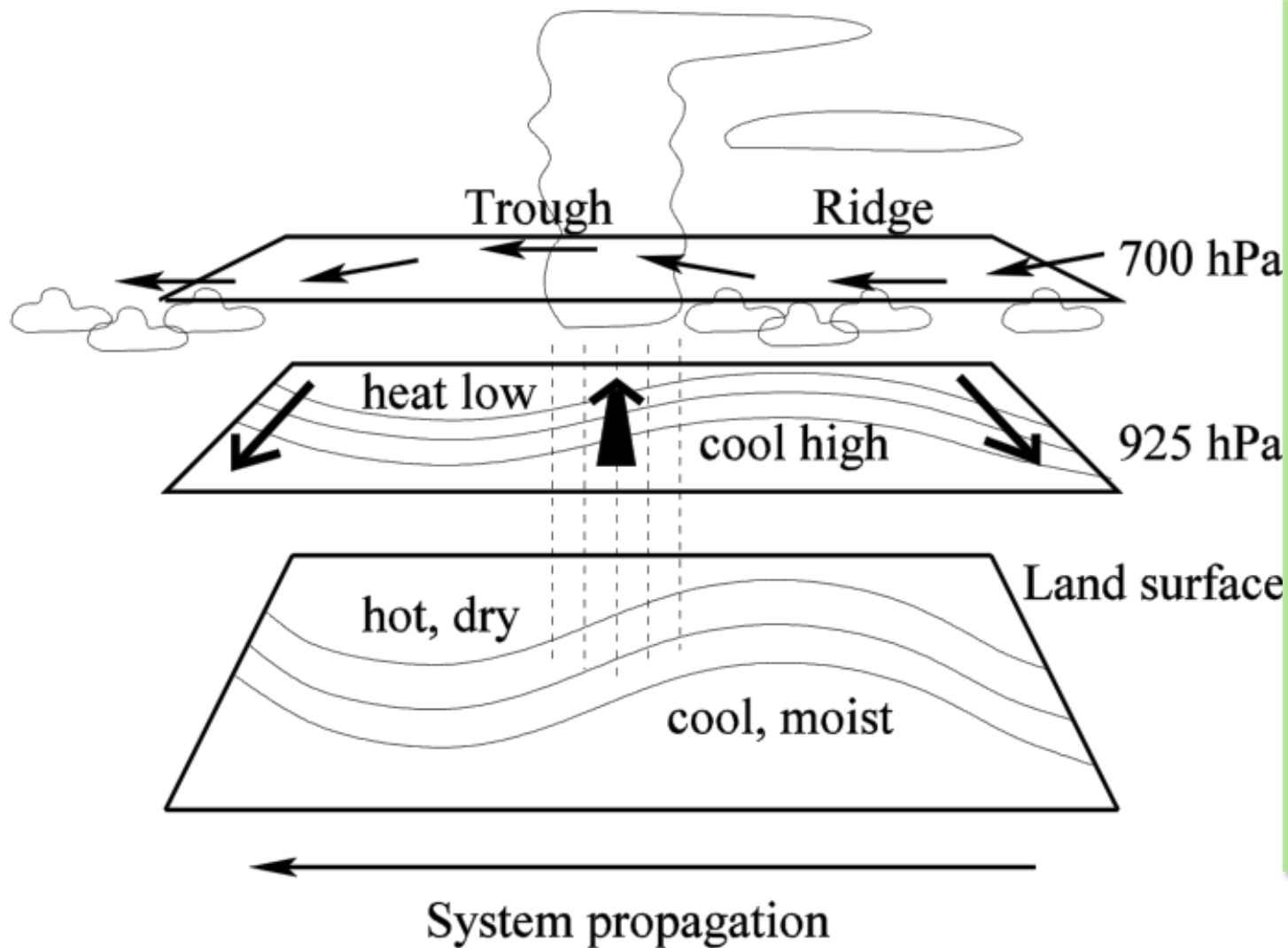


Figure 2.26: Schematic depicting land-atmosphere coupling within an AEW. The modulation of convection by a wave at 700 hPa creates synoptic variability in soil moisture, with wet soils favoured behind the trough. Zonal contrasts in availability of moisture for evapotranspiration drive sensible heat flux patterns, which perturb the isentropes at 925 hPa. Figure 7 from Taylor et al. (2005).

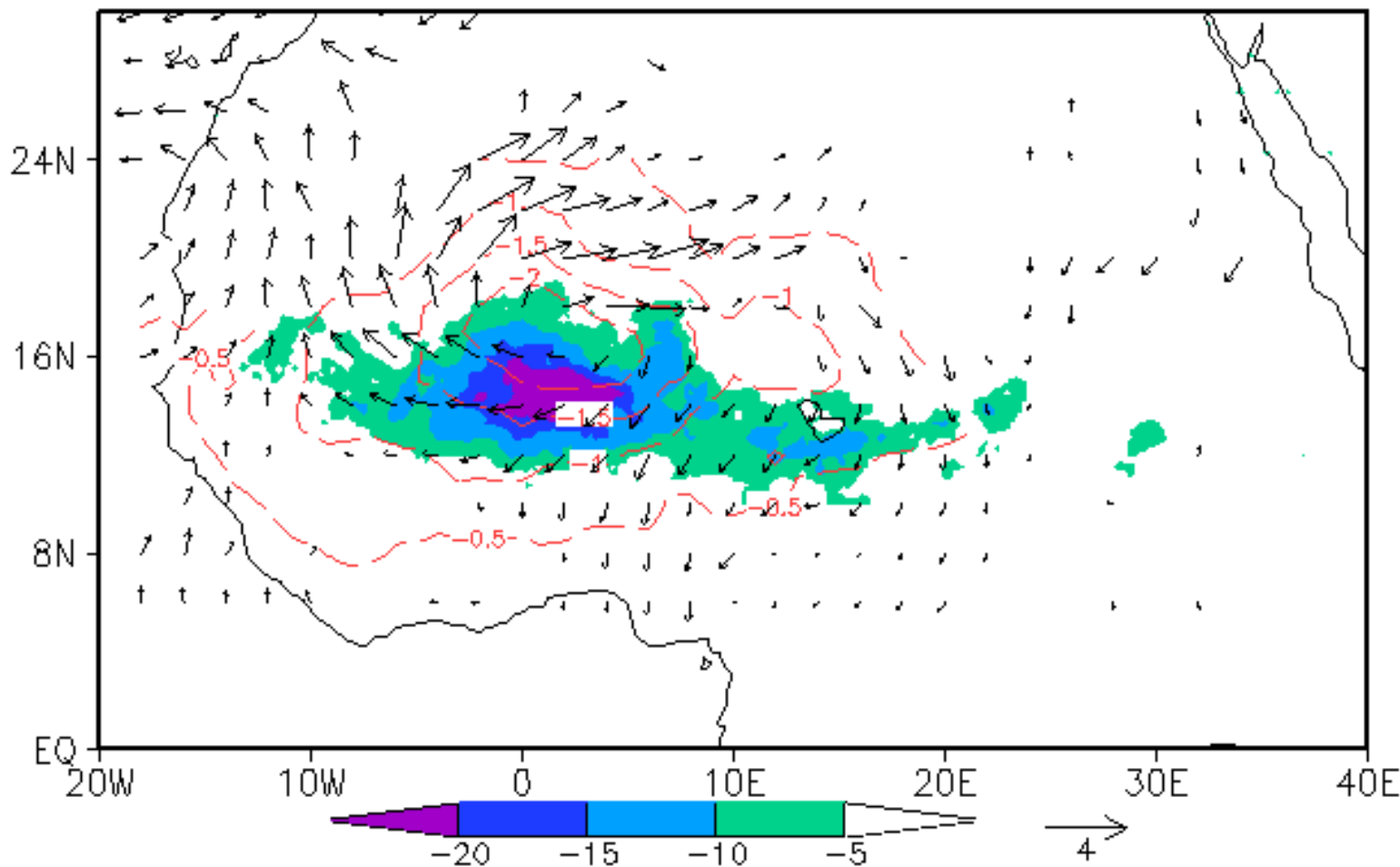
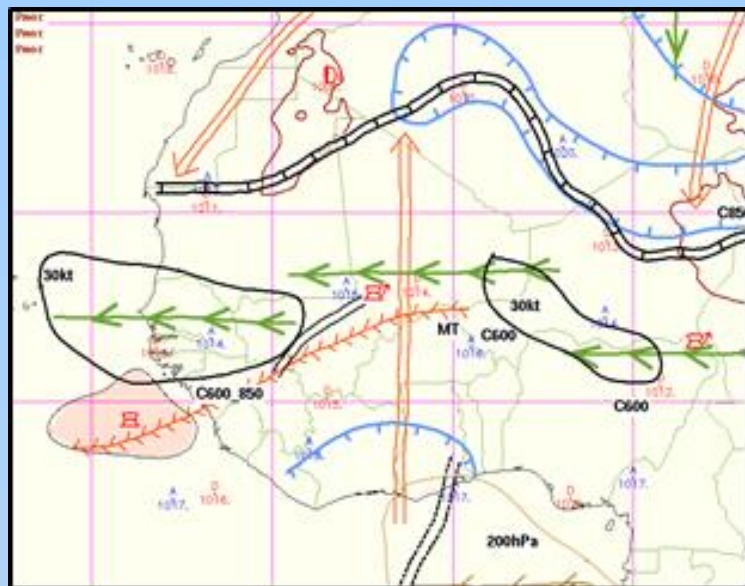


Figure 2.27: Differences in surface sensible heat flux (shaded; Wm^{-2}), 925 hPa temperature differences (at 1800 UTC; dashed contour; K), and wind speed (at 0600 UTC the following day; vectors; ms^{-1}) between wet and dry surface intraseasonal composites. The wet (dry) composite is defined at day 0 by the minimum (maximum) in filtered daytime mean surface heat flux over a rectangle centred on 0°E , 15°N .

Meteorology of Tropical West Africa: The Forecasters' Handbook

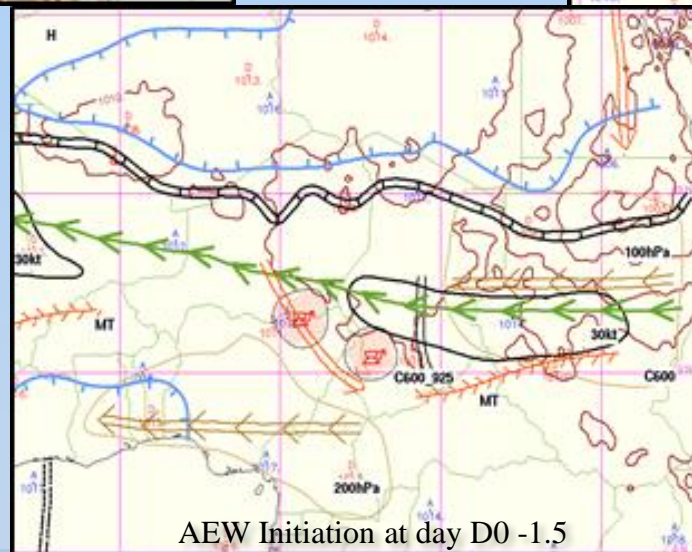
Chapter 2: Synoptic Systems - Lead Authors: R Cornforth, Z Mumba, DJ Parker



AEW arriving at the coast at $D_0 + 1.5$



Mature and growing AEW at day D_0



AEW Initiation at day $D_0 - 1.5$

Figure 2.28: Sequence of WASA charts showing the structure of the AEW of 12-16 August 2012. Day D_0 is 0000 UTC on 15 August 2012. The time sequence is from right to left, in an attempt to be consistent with easterly propagation.

Meteorology of Tropical West Africa: The Forecasters' Handbook

Chapter 2: Synoptic Systems - Lead Authors: R Cornforth, Z Mumba, DJ Parker

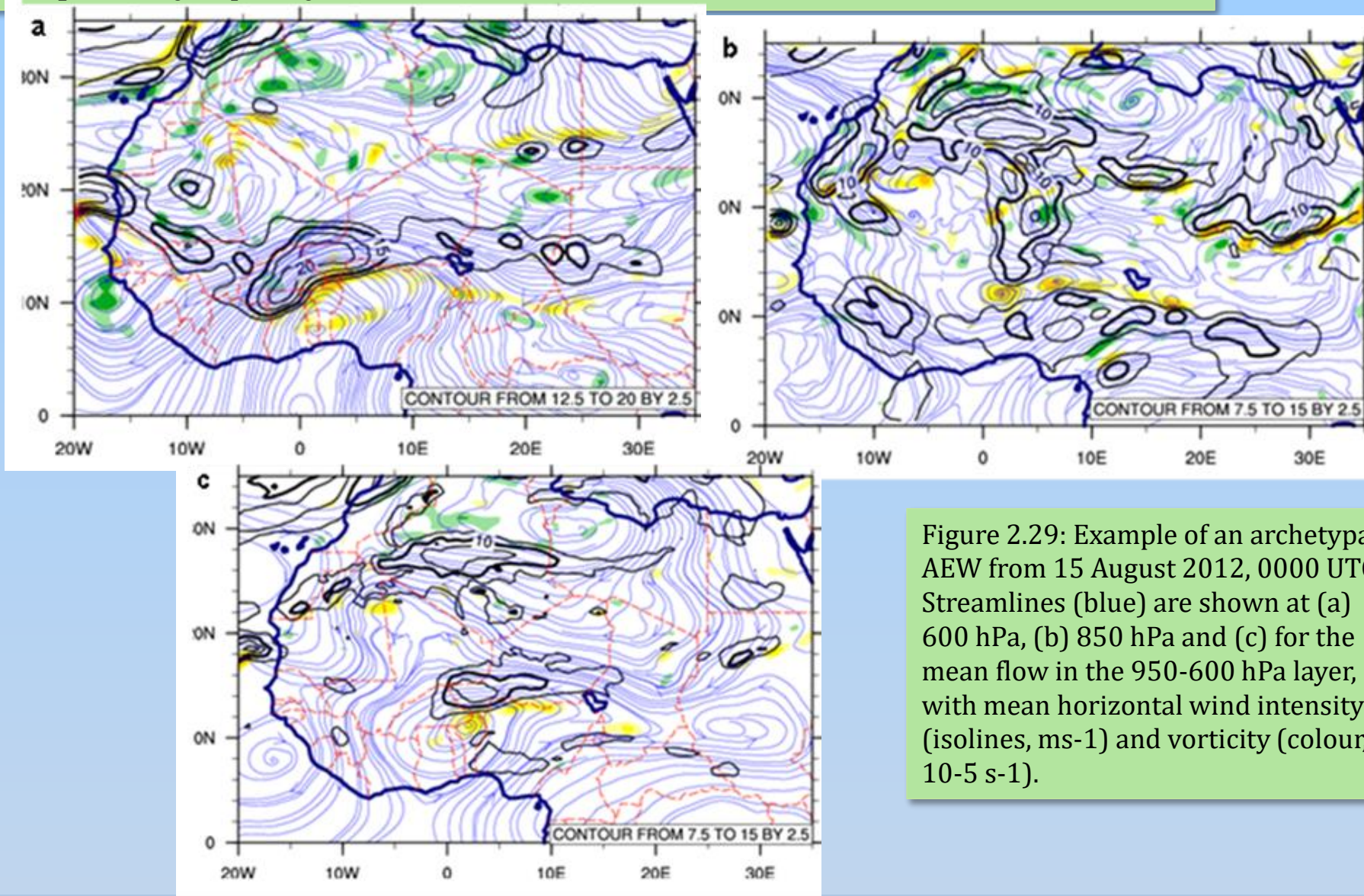


Figure 2.29: Example of an archetypal AEW from 15 August 2012, 0000 UTC. Streamlines (blue) are shown at (a) 600 hPa, (b) 850 hPa and (c) for the mean flow in the 950-600 hPa layer, with mean horizontal wind intensity (isolines, ms⁻¹) and vorticity (colour, 10⁻⁵ s⁻¹).

Meteorology of Tropical West Africa: The Forecasters' Handbook

Chapter 2: *Synoptic Systems* - Lead Authors: R Cornforth, Z Mumba, DJ Parker

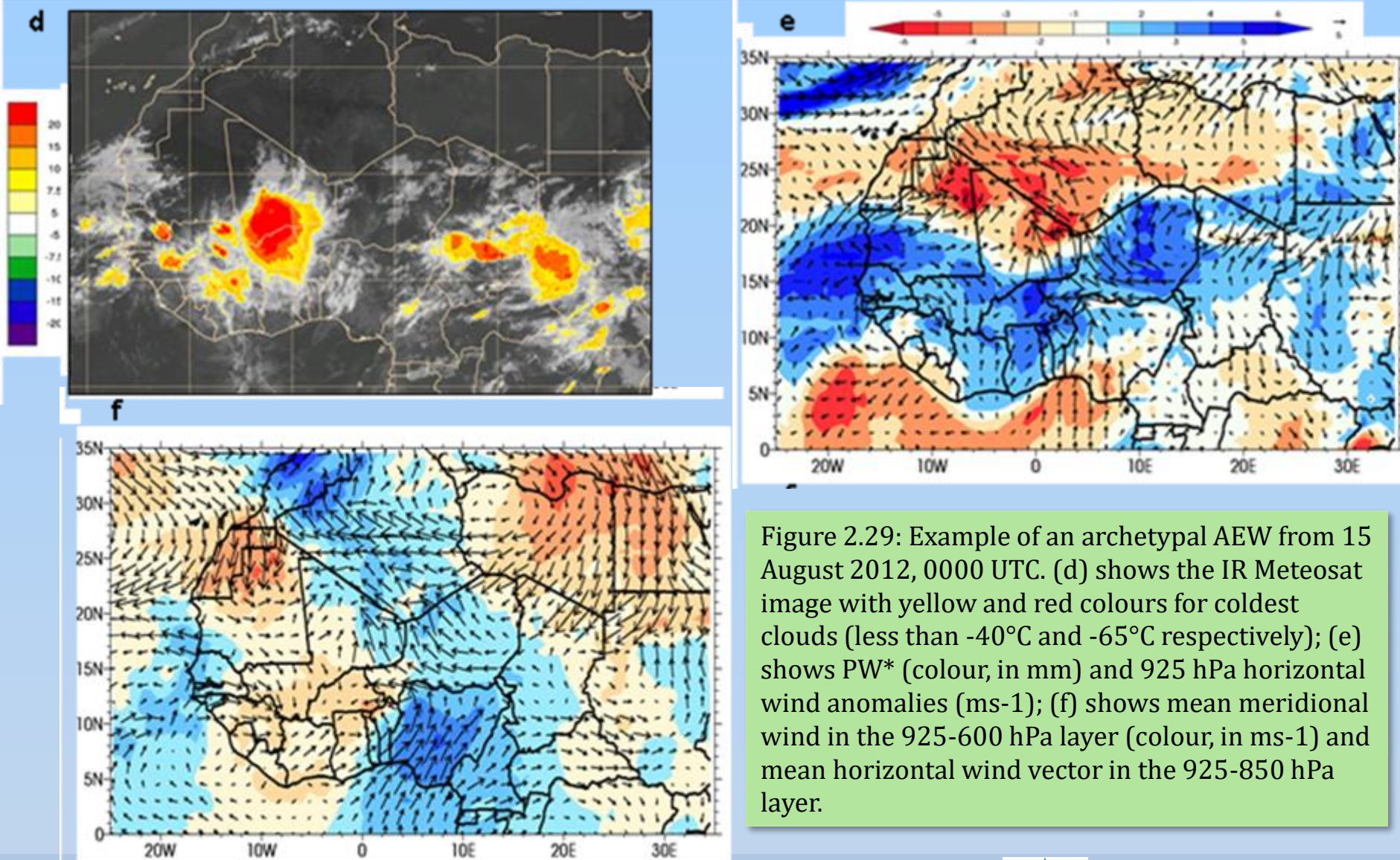


Figure 2.29: Example of an archetypal AEW from 15 August 2012, 0000 UTC. (d) shows the IR Meteosat image with yellow and red colours for coldest clouds (less than -40°C and -65°C respectively); (e) shows PW^* (colour, in mm) and 925 hPa horizontal wind anomalies (ms^{-1}); (f) shows mean meridional wind in the 925-600 hPa layer (colour, in ms^{-1}) and mean horizontal wind vector in the 925-850 hPa layer.

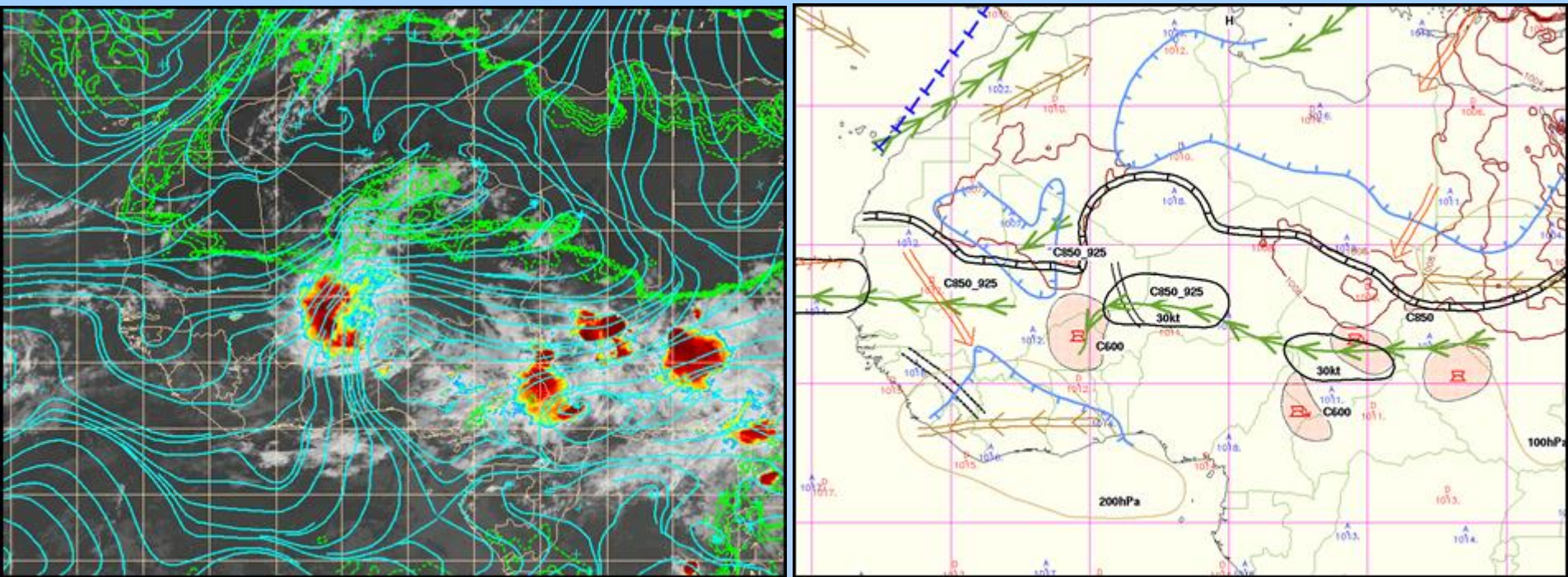


Figure 2.30: Example of an AEW "breaking case" on 7 August 2012 at 0000 UTC (Case study CS01). Left panel shows the IR image with superposition of streamlines at 600 hPa and Td at the surface (green isolines to visualise the ITD); right panel shows the WASA. Note that the breaking of the AEW is identified by the north-south orientation of the streamlines to the west of the trough.

Meteorology of Tropical West Africa: The Forecasters' Handbook

Chapter 2: *Synoptic Systems* - Lead Authors: R Cornforth, Z Mumba, DJ Parker

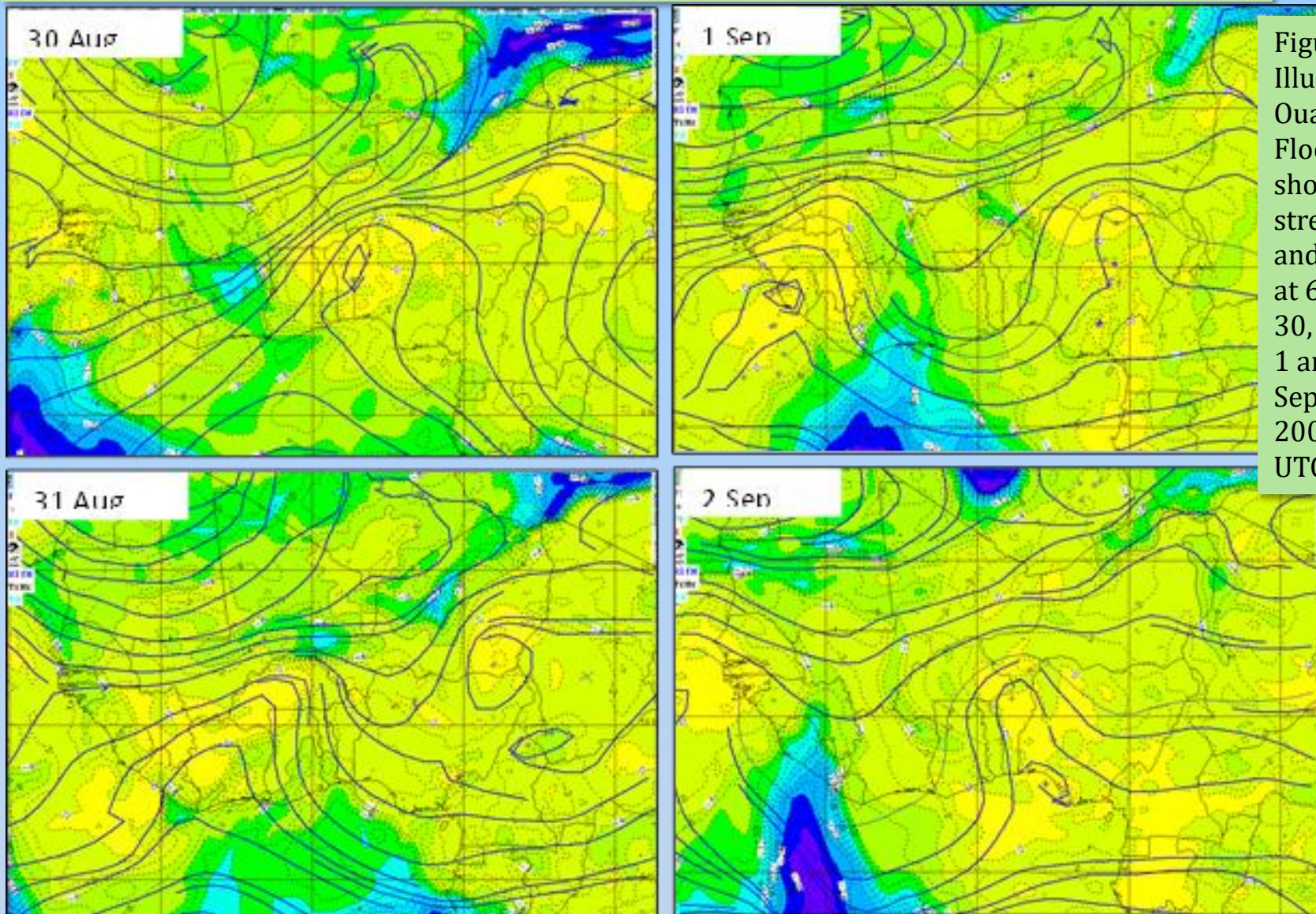


Figure 2.31: Illustration of Ouagadougou Flood case showing streamlines and Td (colour) at 600 hPa on 30, 31 August, 1 and 2 September 2009 at 00:00 UTC.

Meteorology of Tropical West Africa: The Forecasters' Handbook

Chapter 2: Synoptic Systems - Lead Authors: R Cornforth, Z Mumba, DJ Parker

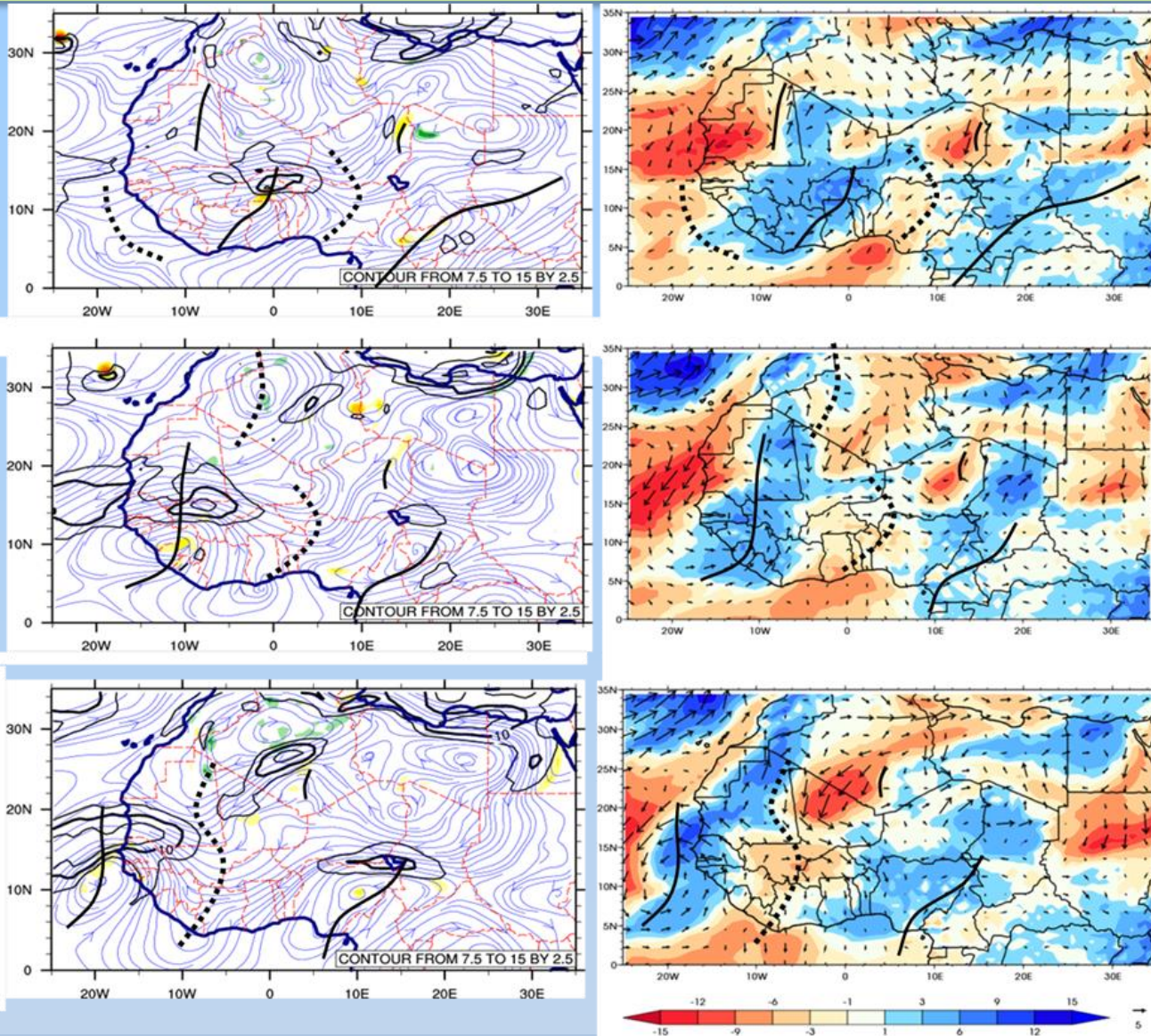


Figure 2.32: Evolution of the synoptic situation on 2, 3, and 4 September 2014 (first, second and third rows respectively) as depicted by the ECMWF analysis at 1200 UTC. *Left column:* streamlines, horizontal wind intensity (2.5 ms^{-1} isoline contours above 7.5 ms^{-1}) and vorticity (colour, in 10^{-5} s^{-1}) for the mean flow averaged in the 950-600 hPa layer. *Right column:* PW^* anomaly (colour, in mm) and 925 hPa horizontal wind anomalies. Trough and Ridge axes as detected by the above diagnostics are superposed by black solid and dashed lines respectively.

Meteorology of Tropical West Africa: The Forecasters' Handbook

Chapter 2: Synoptic Systems - Lead Authors: R Cornforth, Z Mumba, DJ Parker

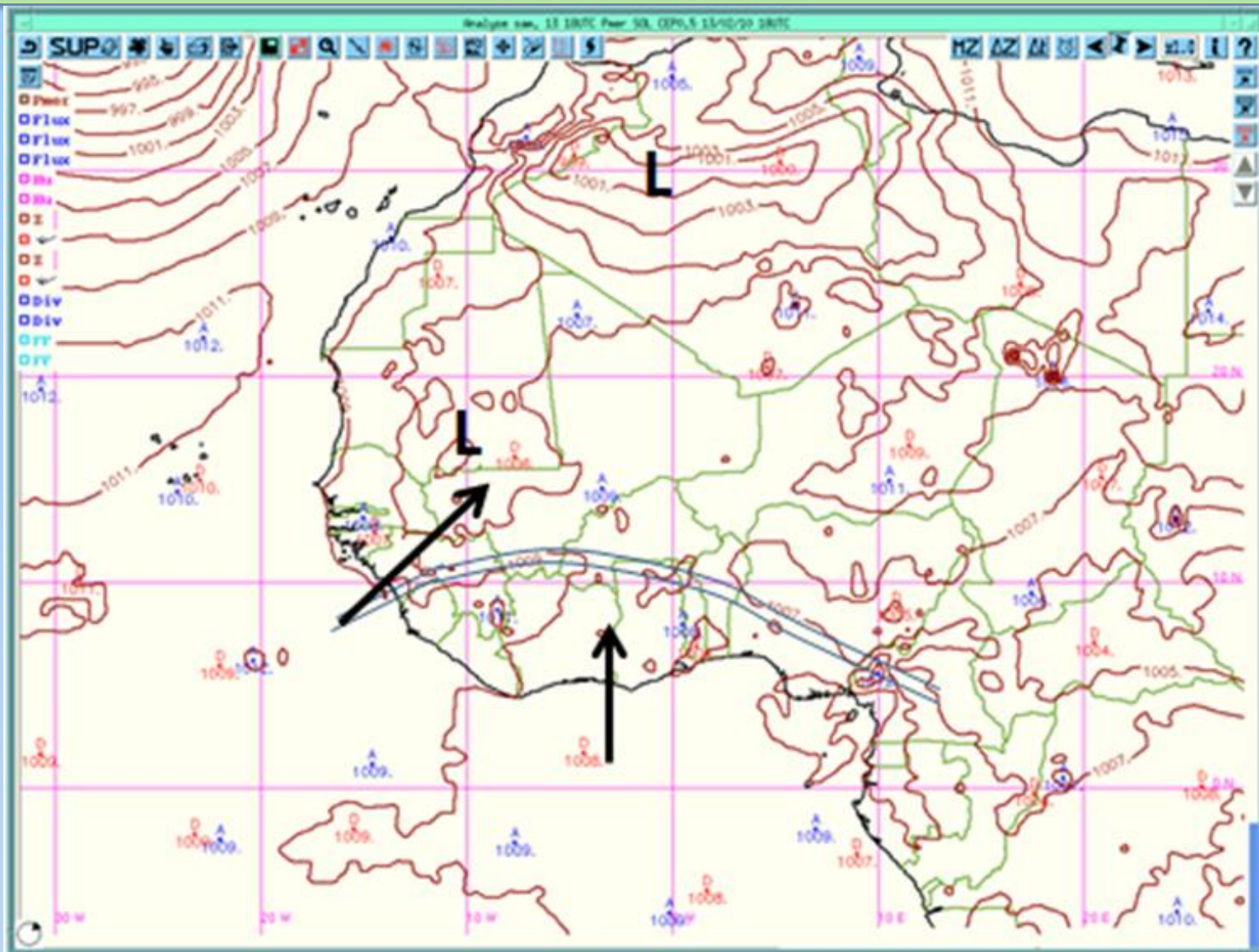


Fig. 2.33 (a) Synoptic situation at 1200 UTC on 13 February 2010, indicating ITD, low level winds (schematic vectors) and trough connecting low pressure systems over Algeria and southern Mauritania.

Meteorology of Tropical West Africa: The Forecasters' Handbook

Chapter 2: *Synoptic Systems* - Lead Authors: R Cornforth, Z Mumba, DJ Parker

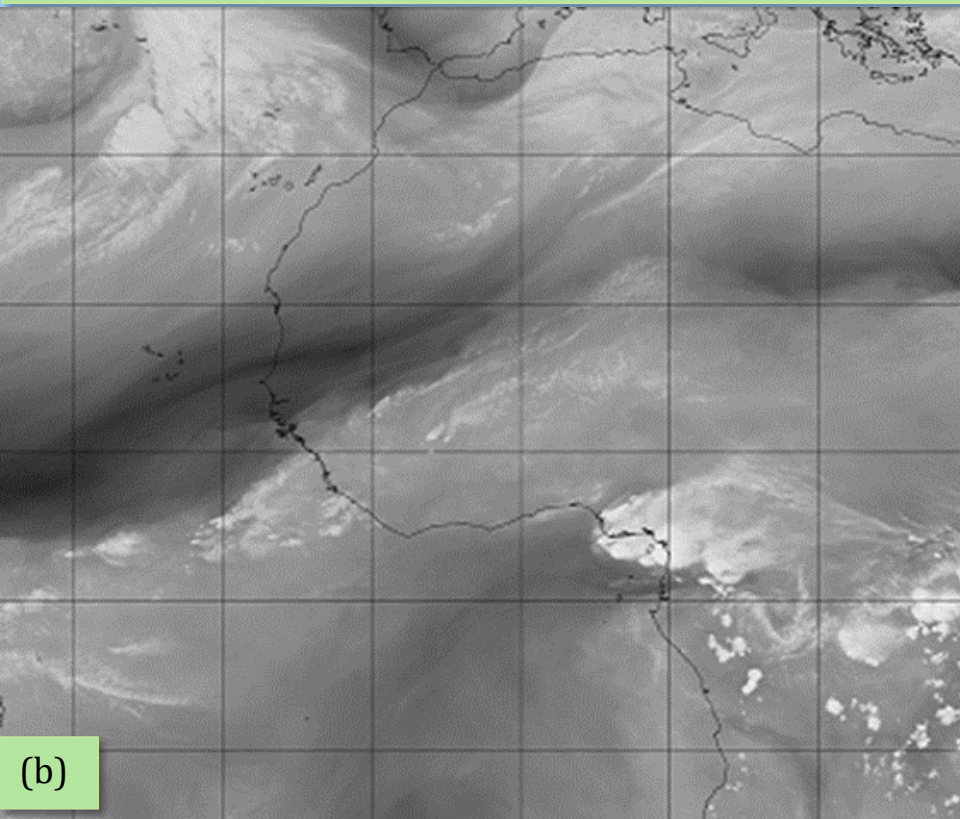


Fig. 2.33 Meteosat SEVERI water vapour imagery at (b) 1200 UTC 13 February and (c) 0000 UTC 15 February 2010.

